Ph.D. Dissertation of Agriculture

Development of a detection system for food hazards by aggregation between gold nanoparticles and aptamer-decorated bifunctional linkers

압타머 성형 이중기능링커와 금나노입자의 응집 기반 식품 내 위해요소 검출 시스템 개발

August, 2021

Eunghee Kim

Department of Agricultural Biotechnology

College of Agricultural and Life Sciences

Seoul National University

농학박사학위논문

Development of a detection system for food hazards by aggregation between gold nanoparticles and aptamer-decorated bifunctional linkers

압타머 성형 이중기능링커와 금나노입자의 응집 기반 식품 내 위해요소 검출 시스템 개발

지도교수 최 영 진

이 논문을 박사학위논문으로 제출함

2021년 8월

서울대학교 대학원

농생명공학부

김웅희

김웅희의 박사학위논문을 인준함

2021년 8월

위 원 장	이 도 엽
부위원장	최 영 진
위 원	강 동 현
위 원	임 석 원
위 원	반 충 진

Abstract

Eunghee Kim

Department of Agricultural Biotechnology

The Graduate School

Seoul National University

The importance of developing analytical methods for rapid detection of harmful microorganisms and harmful substances in the food industry is becoming increasingly prominent as the industry develops. Currently, analysis of hazardous substances is performed through various methods. However, there remains a need for the development of simple, convenient, and rapid detection methods, because the food industry belongs to a relatively low value-added industry and many low-skilled workers are employed.

Gold nanoparticle aggregation based colorimetric detection has been attracting attention due to their simplicity, rapidity, and accuracy. However, it also has a drawback in that it exhibits lower sensitivity compared to electrochemical or optical methods. To overcome these shortcomings, a colorimetric detection method based on a bifunctional linker that exhibits improved visual signals with higher sensitivity has been proposed. However, there were still disadvantages in that the research so far has

been focused on the detection of microorganisms and the diversity of the bifunctional linker is insufficient.

In this study, first, a bifunctional linker-based detection method was applied to detect a new target, Ara h 1, a peanut allergen. The target allergen was rapidly detected below the ED01 threshold, which is the minimum that can be recognized by allergy patients in cookies. By showing that it could detect less than 0.19 mg/mL within 45 minutes, including the extraction time, it was shown that the detection system based on the bifunctional linker can be applied to the detection of various hazards beyond microorganisms. Second, a novel bifunctional linker based on an aptamer, a DNA sequence that could selectively recognize a target, and a colorimetric detection method using this linker were devised. The bifunctional linker was designed by decorating the surface of silica nanoparticles with an aptamer, and on the contrary, for the gold nanoparticles, a DNA sequence complementary to the aptamer was decorated on the surface. In addition, dispersion stability and specific binding ability were imparted through additional surface molding of glutathione. Finally, a detection method for gluten, which induces celiac disease, was developed using a newly designed aptamer based bifunctional linker and gold nanoparticles whose surface was modified with a complementary DNA sequence. Through the development of this detection method, the concentration in the extract of gliadin, a constituent of gluten, was detected up to 0.5 ug/mL by naked eye without an analytical instrument. Although there are still many areas to be studied using the aptamer based bifunctional linker,

this study is expected to pave the way for expanding the scope of application of rapid detection methods based on bifunctional linkers.

Key words: Gold nanoparticle (AuNP), Silica nanoparticle (SNP), Switchable linker (SL), Aptamer

Student Number: 2016-39133

Contents

List of Tables

List of Figures

Chapter I. Literature Review

I-1. Introduction

I-1-1. The necessity of developing a novel detection system for food safety screening

Developments in the food industry have been responding to the rapid increase in food consumption in the modern society. However, at same time, there are more frequent threats to health than before, such as contamination by foodborne pathogens, incorporation of allergens in the process, processed food using ingredients contaminated with heavy metals, pesticide residues, or residual antibiotics, and mycotoxin generation during long-term storage. Under such circumstances, to respond to these many threats, the need has been highlighted to develop rapid, cost-effective, and easy-to-use detection methods to control and monitor food quality and safety incidents in food. [1-3].

Several rapid and accurate instrumental analysis methods have been developed for food quality and safety, such as liquid chromatography (LC) [4], gas chromatography (GC) [5], mass spectrometry (MS) [6], capillary electrophoresis [7], supercritical fluid chromatography [8], GC-MS [9] and LC-MS [10]. These analysis methods have the advantages of high accuracy and sensitivity, however, at the same time, they have the disadvantages of inconvenience, high cost, being time-consuming, and requiring trained operators [11]. For this reason, the development of a new detection method that is simple, inexpensive, and can be used by an untrained person is required in food safety screening.

Table I-1. Develop schedule of detection technology of foodstuff

Technology	Time	Target	Detection Time	Characteristics	References
Colorimetric	1938	Lead	In an hour	Low sensitivity, single sample, large limitation	[12]
Chemiluminescent	1977	S. *marcescens*	3 - 4 h	Simple, wide linear range, dependent on environmental factors	[13]
Colloidal-gold immunoassay	1971	*Salmonellae*	3 - 6 h	Convenient, low cost, wide range, easy to judge false positive	[14]
ELISA	1977	*Staphylococcal Enterotoxin* A	1 -3 h	Simple, specific, easy to false positive, many interference factors	[15]
LC-MS	1986	Heterocydic aromatic mutagens	2-3 h	High sensitivity, poor repeatability, easy interference and narrow range	[16]
Electrochemical sensor	1995	Toxins	Less than 1 h	Good repeatability and stability, low cost, short life	[17]
Nucleic-acid aptamers	1997	Bacterium	4 h	Sensitive, high-throughput, poor repeatability	[18]

I-1-2. Material features of gold nanoparticles in detection method development

With the advancement of nanotechnology in recent decades, a series of new nanomaterials with smart performance have been introduced for a wide range of applications in various fields. Especially, gold nanoparticles, which generally have a particle size distribution between 1 nm and 100 nm, are very stable nanomaterials that have been extensively studied and applied [19-21]. Due to its unique physicochemical properties, gold nanoparticles have been used in chemical energy, electronic devices, environmental monitoring, biomedical and food safety monitoring. Its beneficial electronic, catalytic, chemical, and optical properties make it popular in research in biochemical sensing technologies, immunoassays, electrochemical analyses, and biomedicine. The surface plasmon resonance properties of gold nanoparticles shift the maximum characteristic absorption peak wavelength in the UV-visible region with changes in particle size, shape and interparticle distance, and is accompanied by a color change [22, 23]. Gold nanoparticles can be used to establish optical sensing techniques using aggregation (or disaggregation) of nanoparticles induced by the formation of covalent or non-covalent bonds with target substances. A solution of gold nanoparticles changes from wine red to blue due to their aggregation, and the surface plasmon band shifts from 523

nm to 610 to 670 nm are observed [24-26]. In addition, multiple hazards in food can be detected using functional gold nanoparticles based on agents triggered by target analytes. A colorimetric sensor based on gold nanoparticles is simple, fast, sensitive, and has been widely applied in real-time field monitoring and rapid testing of food quality and safety.

I-1-3. Methods for the synthesis of gold nanoparticles

The preparation methods of gold nanoparticles are mainly divided into physical and chemical methods. As for the physical method, various approaches such as vacuum condensation, electrical dispersion, ultrasonication, and laser ablation [27] have been studied, but they are generally less preferred because of their complexity and relative non-uniformity in particle size. Chemical methods include citric acid reduction, the sulfhydryl ligand method, seed crystal growth, and electrochemical and photochemical methods [28]. Through these methods, gold nanoparticles with diameters ranging from 2 nm to 150 nm and with various shapes, including nanospheres, nanorods, nano shells and nano cages, can be rapidly synthesized. In terms of the current gold nanoparticle based colorimetric sensors, the most widely applied shape of gold nanoparticle is a sphere, and its synthesis is mainly achieved by chemical synthesis methodologies introduced by

Turkevich in 1951 and further developed by Frens in 1973 [29, 30]. Citric acid reduction, also known as the Turkevich–Frens method, is a simple water-phase oxidation-reduction method. First, a chloroauric acid solution of a certain concentration (typically, 1 mM) is boiled, and a certain amount of sodium citrate solution (typically, 38.8 mM) is added. The Au (III) is reduced and aggregates to forms gold seeds. Through electrostatic interactions, ions (H^+, $AuCl_4^-$) adsorb on the surfaces of the gold seeds to form a stable colloidal gold solution (diameter of 13 nm). Citrate, used as the reducing agent, plays a role in imparting dispersion stability on the surface of gold nanoparticles. The method is simple, and the prepared gold nanoparticles are well dispersed with a uniform particle size distribution. The particle size is affected by the ratio of chloroauric acid to sodium citrate and can be controlled within 3–100 nm by changing the ratio [31]. Additionally, there is a method developed by Brust-schiffrin for synthesizing smaller-sized gold nanoparticles. The Brust-Schiffrin method is a classic sulfhydryl ligand method that uses tetra-n-octyl ammonium bromide as a medium to transfer chloroauric acid from the aqueous phase to the organic phase. Then $NaBH_4$ and thiol are used as reducing agents and ligands instead of citrate, respectively, to prepare gold nanoparticles. Tetra-n-octyl ammonium bromide can be used as a phase

transition and stabilizer to protect gold nanoparticles [32]. This method is an easy approach that allows for the synthesis of thermally- and air-stable gold nanoparticles ranging in diameter from 1–8 nm. In the seed growth method, small gold nanoparticles prepared by water phase redox are used as seeds, chloroauric acid solution is used as the growth solution, and $HAuCl_4$ is reduced on the surface of gold nanoparticles to produce large gold nanoparticles [33].

I-1-4. Optical property of gold nanoparticles

Because of their small size, gold nanoparticles have unique physicochemical properties, good optical properties, high electron density, good biocompatibility, catalytic performance, etc [34]. This is because the motion of electrons becomes limited by the size of nanoparticles, and interactions are expected to be mostly on the surface due to the high surface-to-volume ratios. Among the various optical properties, surface plasmon resonance [34] and fluorescence quenching [35, 36] are the most commonly exploited optical properties. Surface plasmon resonance occurs when the vibrational frequency of free electrons interacts with the frequency of incident light to generate a resonance coupling [37]. This results in strong characteristic absorption for gold nanoparticles in the UV-visible region. The maximum

absorption wavelength depends on changes in the size, shape, and distance of the gold nanoparticles [38]. For example, the surface plasmon band peaks of spherical gold nanoparticles with average diameters of 9, 15, 48 and 99 nm were observed at 517, 520, 533 and 575 nm, respectively. As the gold nanoparticle diameter increases, the surface plasmon band undergoes an obvious red shift [39].

I-1-5. Functionalization of gold nanoparticles

Because gold nanoparticles have the unique optical properties mentioned above, they can be formed into transducer moieties that convert their sensing behavior into eye-sensitive color changes. However, further development of gold nanoparticle-based sensors with high selectivity and sensitivity requires a functionalization step that introduces gold nanoparticles into recognition motifs that can promote specific responses to the analyte under investigation. Molecular modification on the surface of gold nanoparticles increases stability, and improves physicochemical properties and functions, which can be used for more biological and chemical reactions, thereby expanding the scope of application. Current surface modification methods use electrostatic absorption, covalent bonding, or attachment of small molecules or compounds for specific

recognition of the target [40]. Electrostatic absorption, covalent bonding, and specific recognition are the three methods commonly used to attach specific motifs to the surface of gold nanoparticles.

For the electrostatic absorption method, the basic principle is the attraction between oppositely charged species. It is a rather straightforward process that has the advantage of saving time and reducing the complexity of preparing ligands. However, the driving force in incorporating charge recognition motifs comes from electrostatic interactions. The binding stability between the motif and gold nanoparticles is highly dependent on solution parameters, such as pH value and salt concentration. Changing these parameters can lead to separation of motif ligands [41]. Compared to electrostatic immobilization, covalent bonding provides high stability for gold nanoparticles, so it can withstand high salt concentration, heat treatment and attack of other molecules. Good properties come from the strong affinity between thiol groups and the gold atoms. In particular, the sulfur atom of the thiol contributes a long electron pair to the empty orbital of the gold atom at the interface, which forms the basis for the bonding of the thiol motif and gold nanoparticles. To date, numerous thiol derivatives or thiol-modifying molecules such as glutathione, thioether, dithiocarbamate alkane thiolate,

DNA peptides, and proteins have been reported for the generation of functionalized gold nanoparticles. The recent introduction of thiol-modified aptamers into gold nanoparticles has attracted great interest, because aptamers are single-stranded DNA or RNA molecules with high affinity and specificity for target analytes. Specific recognition is based on the principle of the explicit specificity of a ligand molecule for an assay molecule, such as gold nanoparticles labeled with an antibody and used for antigen detection [42].

I-2. Gold nanoparticles based colorimetric detection systems

I-2-1. Principle of gold nanoparticles based colorimetric detection systems

The fundamental mechanism of gold nanoparticle-based colorimetric sensor fabrication relies primarily on surface plasmon resonance as its dependence on distance. Aggregation of appropriately sized gold nanoparticles induces surface plasmon resonance bonding and causes color change in the visible region. Electromagnetic coupling of gold nanoparticles has been found to be effective when the interparticle distance is less than 2.5 times the individual diameter [43]. In particular, the state of the various gold nanoparticles in solution exhibits a distinct color. Gold nanoparticles dispersed in solution have a red color with maximum absorption at ~520nm. On the other hand, when gold nanoparticles agglomerate, the surface plasmon bands move from the visible region to the near-infrared region by agglomeration, thereby changing the color of the solution from red to blue or violet. Conversely, redistribution of agglomerated gold nanoparticles causes a color change from purple or blue to red. In general, zero-charged bare gold nanoparticles tend to agglomerate due to van der Waals attraction, which is why a stabilization step is required in gold nanoparticle synthesis. To date, a common approach to

stabilize gold nanoparticles is to electrostatically or sterically use a variety of surface ligands. Therefore, the aggregation and redispersion behavior of gold nanoparticles is highly dependent on the surface microenvironment, which can be initiated by changes in the external environment [44]. These properties of gold nanoparticles were used for colorimetric analysis. The stability of gold nanoparticles can be hindered or maintained when adding analytes. Based on this theory, two basic strategies (aggregation or anti-aggregation) have been explored for the colorimetric detection of target molecules by gold nanoparticles.

I-2-1-1. Analysis based aggregation of gold nanoparticle.

In the simplest form of aggregation-based detection system, interparticle aggregation of gold nanoparticles triggered by analytes is a key point in preparing this type of sensor, which is usually a specific interaction between the analyte and gold nanoparticles. It is achieved by introducing and utilizing nature. However, these direct interactions are rather difficult to provide for a wide range of applications, as the multiple binding sites and high affinity for gold nanoparticles imparted by the analyte are highly dependent on the intrinsic structure. Fortunately, after the gold nanoparticles are

functionalized, certain interactions between the functional groups of the gold nanoparticles and the analytes are carried out, so that the aggregation of gold nanoparticles can be developed into a series of colorimetric assays for various molecular analysis [45]. Various molecules such as DNA, antibodies, small molecules, and metal ions can be analyzed using the concepts mentioned above so far [46]. Certain ligands are required for the functionalization of gold nanoparticles. In general, one end of a ligand should have a sulfhydryl group and the other end should have a functional group capable of binding to the target. The sulfhydryl group of the ligand can bind to the surface of gold nanoparticles through strong Au-S bonds [47]. In the presence of the target compound, the ligand binds to the target compound, reducing the distance between the gold nanoparticle particles and causing aggregation [48].

I-2-1-2. Analysis based anti-aggregation of gold nanoaparticle.

In the anti-aggregation system, the model molecules (or linkers) induce aggregation by cross-linking gold nanoparticles via the formation of linkages. However, the recognition of analyte could change the state of the linker. And, through the regulation of the linker state, the control of the aggregation behavior of gold nanoparticle can also be achieved. Heavy metal

ions, melamine, or pesticide residues can be detected in food by using the principle of the blocking of gold nanoparticle aggregation. [49-53]

I-2-2. Application of gold nanoparticles detection systems in food safety.

I-2-2-1. microorganisms

Molecular biology techniques are highly sensitive, but time consuming and require a high level of technical expertise and expensive reagents. Direct detection of microorganisms using properly functionalized AuNPs provides a simple and direct alternative diagnostic method. Targets can be captured with specific aptamers, antibodies, or selective organic metals immobilized on AuNPs. Ma et al. developed a GNP apta sensor to detect *Salmonella* Typhimurium, a common cause of food-related diseases [54]. An aptamer is a short specific oligonucleotide or single-stranded DNA (ssDNA) sequence. They are absorbed on the surface of the GNP and prevent aggregation of the GNP. However, in the presence of a specific target, the aptamer preferentially desorbs from GNP and binds to the target, causing GNP aggregation. Du et al. demonstrated the ability to detect *Listeria monocytogenes* using OLG-GNP (oligonucleotide-functionalized GNPs) as detection probes [55]. This colorimetric assay requires bacterial DNA

extraction and amplification of the *hlyA* gene from *L. monocytogenes* (corresponding to the OLG probe) via PCR prior to analysis. Upon addition of OLG-GNP, the presence of the PCR product *hlyA* gene or target genomic DNA prevented aggregation of GNPs, while negative samples resulted in aggregation and a colorless solution that was easily detected with the naked eye. The detection limits were 48.4 and 100.4 ng, respectively, and a low-cost bacterial sensor for *E. coli* O157:H7 analysis was reported as a Gram-negative bacterial detection model using mercaptoethylamine-modified AuNPs (MEA-AuNPs). MEA molecules bind to *E. coli* O157:H7 through electrostatic adhesion between the positive charge of MEA and the negative charge of *E. coli* O157:H7, and MEA-AuNP can crosslink in the presence of a certain amount of *E. coli* O157: H7 which brings a dramatic color shift from red to blue. The absorbance ratio (A625/A520) of the modified AuNP showed a linear correlation with the *E. coli* O157:H7 concentration [56]. Although most GNP colorimetric assays require sample concentration prior to analysis, Thiramanas and Laocharoensuk have demonstrated a strong electrostatic interaction of positively charged polyethyleneimine coated GNP (PEI-GNP) and negatively charged enzyme (β-galactosidase). Bacteria generate competitive binding assays to eliminate this step. The binding of the enzyme to PEI-GNP inhibits its activity, but in the presence of large amounts of

bacteria, PEI-GNP preferentially binds to the LPS of Gram-negative bacteria (e.g., enterotoxic *E. coli*) or Teicosan in Gram. Positive bacteria (*S. aureus*) and enzyme activity are restored. Enzyme activity can be monitored colorimetrically through the hydrolysis of the substrate chlorophenol red β-D-galactopyranoside, which can be visually detectable within 10 minutes using a UV-vis spectrophotometer or within 2-3 hours, with an apparent yellow to red color. This assay has been successfully applied to drinking water samples to detect both Gram-positive and Gram-negative bacteria with a detection limit of 10 CFU mL^{-1} [57].

I-2-2-2. Microbial toxins

Even if live pathogens are no longer present, there is the question of toxins that might be left behind by the pathogen. In particular, endotoxins and exotoxins could play a role during the outbreak of foodborne diseases [58]. An endotoxin is found in gram negative bacteria. This toxin is located at the lipid part of lipopolysaccharide (LPS) and may be released if the bacterium dies. In contrast, an exotoxin can be released from living bacterial cells. For example, Staphylococcus aureus can release a food poisoning exotoxin known as staphylococcal enterotoxin [59], and Listeria monocytogenes produces and

releases listeriolysin O which acts as a hemolysin that has an ability to destroy red blood cells [60]. In the last decade, multiple rapid and sensitive screening methods for monitoring food toxins were introduced, including bioassays, gelcoat technique, turbidimetric technique as well as mass spectrometry-based methods [61, 62]. Gold nanoparticle-based colorimetry as an alternative diagnostic platform has attracted tremendous attention recently.

Apart from the specific decorator-gold nanoparticle platforms, another powerful method that shows high sensitivity and selective detection for a target toxin is based on the immunoassay. So far, many kinds of antibody-gold nanoparticle-based systems allow for the specific monitoring of numerous toxins, such as microcystin-LR toxin, aflatoxin B1, ochratoxin A, cholera toxin, zearalenone [63-67]. All these proposed immunoassays provide a promising approach for rapid, highly-selective, and cost-effective monitoring of toxins in the field of food safety. Direct electrostatic aggregation of gold nanoparticles has been explored for the monitoring of toxins. For example, negative charged aptamers could make gold nanoparticles stable and dispersed against salt-induced aggregation due to the introduction of electrostatic repulsion [68]. Additionally, aptamer-modified gold nanoparticles were developed to detect aflatoxin B2 with the LOD of 25

pg/mL [69].

I-2-2-3. Chemical hazards

Chemical hazards include heavy metals, pesticide residues, drug residues etc. They all have long played a very important role in agriculture by protecting crops and improving productivity, but inappropriate pesticide spraying can accumulate in crops, food, and food by-products [70, 71], which is a health and international trade issue [72]. Therefore, the government has set a safe maximum residual limit for various chemicals. Since chemical hazards are present in very small amounts, the detection method must be very sensitive and selective. Therefore, the ability to monitor low concentrations of these compounds is of particular importance. With the increasing understanding of the properties of gold nanoparticles in recent years, many types of gold nanoparticle-based sensors have been reported for the detection of various chemical hazards.

In the case of metal detection, oligonucleotide or DNA functionalized gold nanoparticles are a powerful diagnostic platform. For instance, by taking advantage of the complementary nature of the DNA or oligonucleotide and

thymine-Hg^{2+}-thymine (T-Hg^{2+}-T) coordination chemistry [73], a complementary DNA-gold nanoparticle system with designed and T-T mismatches has been introduced for Hg^{2+} detection [74, 75].

Proteins or oligopeptides are rich in highly specific ligands enabling the capture of specific targets through their functional groups at the inner or outer surface. For metal ions, coordination to cysteine is the dominant mechanism for metal-protein or metal-oligopeptide incorporation. Based on the strong affinity of heavy metal to thiols, papain with seven cysteine residues was functionalized on gold nanoparticles as the recognizing moiety, and this diagnostic platform could be used to simultaneously detect Hg^{2+}, Pb^{2+} and Cu^{2+} based on the mechanism that these metals can induce the aggregation of the as prepared gold nanoparticles [76]. Furthermore, a self-assembly of gold nanoparticles core-satellite structure modified with naturally occurring tripeptide glutathione as linker was designed for Pb^{2+} detection, and the limit of detection (LOD) can reach 9.9 ppb with high selectivity against other heavy metals [77].

One of the most used strategies is for target pesticide residues to induce agglomeration of gold nanoparticles or modified gold nanoparticles. For example, Bai and his team have developed a sensitive optical sensor for

screening fimetogens based on their ability to rapidly induce agglomeration of gold nanoparticles. The concentration of pimetrogen can be measured visually with a detection limit of less than 1 μM, and this system exhibits a higher selectivity for pimetrogen than 11 other pesticides [45]. In addition, we developed a colorimetric assay for the detection of six organophosphorus pesticides by selecting organophosphorus pesticide aptamers using ssDNA absorption on the surface of gold nanoparticles. If the target pesticide is present in the system, the organophosphorus pesticide aptamer specifically binds to the pesticide, and this binding separates the pesticide from the gold nanoparticles, ultimately causing a color change from red to violet-blue due to agglomeration of the gold nanoparticles [78]. In addition, a new system including unmodified gold nanoparticles, aptamers, and positively charged PDDA has been introduced to detect malathione. In this colorimetric assay, PDDA can bind with the aptamer through the electrostatic attraction between the cationic PDDA and the negatively charged phosphate backbone of the aptamer. Therefore, aggregation of gold nanoparticles is prevented. However, in the presence of malathione, aptamers form a complex with malathione, freeing PDDA and leading to agglomeration of gold nanoparticles [79].

Table I-2. Developed detection methods by type of food contaminants

Type of food contaminants	Analytes	Functionalization of gold nanoparticle and strategy	Limit of detection	References
microorganisms	*Campylobacter jejuni*	Unmodified; Aggregation	7.2×10^5 CFU/mL	[80]
	ETEC, *S. areus*	Polyethyleneimine modified; Anti-aggregation	10 CFU/mL	[57]
	Listeria monocytogenes	ssDNA; Anti- aggregation	100.4 ng of genomic DNA	[55]
	Baciluus cereus	Unmodified; Aggregation	9.2×10^1 CFU/mL	[81]
Food toxins	Cholera toxin	Lactose modified; Aggregation	3 µg/mL	[82]
	Ricin	Sugar modified; Aggregation	10 pg/mL	[83]
	Aflatoxin B1	Antibodies modified; SPR absorption	12 ng/L	[66]
	Zearalenone	Antibodies modified; SPR absorption	2.5 ng/mL	[65]

Type of food contaminants	Analytes	Functionalization of gold nanoparticle and strategy	Limit of detection	References
Heavy metals	Hg^{2+}	ssDNA; Aggregation	~10 nM	[84]
	Hg^{2+}	Unmodified; Anti-aggregation	10 nM	[85]
	Pd^{2+}	Tripeptide glutathione; Aggregation	47.6 nM	[77]
	Hg^{2+}, Pb^{2+} and Cu^{2+}	Papain; Aggregation	200 nM	[76]
Pesticide drug resiues	Organophosphorous	Unmodified; Anti-aggregation	~3 ppm	[78]
	Malathion	Unmodified; Anti-aggregation	0.06 pM	[79]
	Imidacloprid	Ionic liquid modified; Aggregation	5×10−7M	[86]
Hazardous organic substances	Melamine	Unmodified; Aggregation	0.05 mg/L	[87]
	Melamine	MA-modified; Aggregation	0.4 μg/mL	[88]
	Melamine	Unmodified; SPR absorption	0.08 ppb	[89]

I-3. Motivation and Aims of the Dissertation

In the past decades, colorimetric detection methods have been developed to detect hazardous factors in foods using aggregation or disaggregation of gold nanoparticles. One of proposed method is a colorimetric detection method that applies the concept of a switchable linker that has the function of inducing large-scale aggregation of gold nanoparticles, and in this way loses this aggregation ability when the detection target is recognized. This detection method has the advantages of high sensitivity and selectivity, fast detection speed, and better visual confirmation by using a precipitation reaction rather than a change in color. Despite these advantages, there were areas that needed to be developed. First, despite the existence of several types of detection targets, studies so far have mainly focused on the detection of microorganisms in food. Second, it was difficult to diversify detection targets by using an antibody-based switchable linker, and refrigerated storage and high manufacturing cost were required.

This dissertation aimed to develop a novel colorimetric detection system for food safety using a switchable linker by presenting experimental results from three key areas.

First, a detection method was developed to quickly and easily detect Ara h1, a major peanut allergen in food, using an antibody-based switchable linker.

Second, I developed a new switchable linker that could replace the antibody-based switchable linker by modifying aptamers, DNA fragments, on silica nanoparticles. A complementary gold nanoparticle was also developed that could react with an aptamer-based linker to form aggregates.

Third, a novel colorimetric detection method was developed for gluten detection, which causes celiac disease, using the above aptamer-based switchable linker and complementary gold nanoparticles.

I-4. References

1. Bansal, S., et al., Food adulteration: Sources, health risks, and detection methods. *Critical reviews in food science and nutrition*, 2017. 57(6): p. 1174-1189.
2. Chiu, Y.-H., et al., Association between pesticide residue intake from consumption of fruits and vegetables and pregnancy outcomes among women undergoing infertility treatment with assisted reproductive technology. *JAMA internal medicine*, 2018. 178(1): p. 17-26.
3. Ortelli, D., A.S. Spörri, and P. Edder, Veterinary drug residue in food of animal origin in Switzerland: a health concern? *CHIMIA International Journal for Chemistry*, 2018. 72(10): p. 713-717.
4. Dias, A.N., et al., Use of green coating (cork) in solid-phase microextraction for the determination of organochlorine pesticides in water by gas chromatography-electron capture detection. *Talanta*, 2015. 134: p. 409-414.
5. Liu, G., et al., Preparation of a magnetic molecularly imprinted polymer using g-C3N4–Fe3O4 for atrazine adsorption. *Materials Letters*, 2015. 160: p. 472-475.
6. La Torre, G.L., et al., Direct determination of phenolic compounds in Sicilian wines by liquid chromatography with PDA and MS detection. *Food Chemistry*, 2006. 94(4): p. 640-650.
7. Omar, M.M.A., A.A. Elbashir, and O.J. Schmitz, Capillary electrophoresis

method with UV-detection for analysis of free amino acids concentrations in food. *Food chemistry*, 2017. 214: p. 300-307.

8. Jin, C., et al., Supercritical fluid chromatography coupled with tandem mass spectrometry: A high-efficiency detection technique to quantify Taxane drugs in whole-blood samples. *Journal of separation science*, 2017. 40(19): p. 3914-3921.
9. Wang, H., et al., Analysis of organochlorine pesticides in surface water of the Songhua River using magnetoliposomes as adsorbents coupled with GC-MS/MS detection. *Science of the Total Environment*, 2018. 618: p. 70-79.
10. Malachová, A., et al., Advanced LC–MS-based methods to study the co-occurrence and metabolization of multiple mycotoxins in cereals and cereal-based food. *Analytical and bioanalytical chemistry*, 2018. 410(3): p. 801-825.
11. Liu, G., et al., Determination of triazole pesticides in aqueous solution based on magnetic graphene oxide functionalized MOF-199 as solid phase extraction sorbents. *Microporous and Mesoporous Materials*, 2018. 270: p. 258-264.
12. Perlman, J., Rapid Colorimetric Determination of Lead in Maple Syrup. *Industrial & Engineering Chemistry Analytical Edition*, 1938. 10(3): p. 134-135.
13. Halmann, M., B. Velan, and T. Sery, Rapid identification and quantitation of small numbers of microorganisms by a chemiluminescent immunoreaction. *Applied and environmental microbiology*, 1977. 34(5): p. 473-477.
14. Faulk, W.P. and G.M. Taylor, Communication to the editors: an immunocolloid

method for the electron microscope. *Immunochemistry*, 1971. 8(11): p. 1081-1083.

15. Saunders, G.C. and M.L. Bartlett, Double-antibody solid-phase enzyme immunoassay for the detection of staphylococcal enterotoxin A. *Applied and environmental microbiology*, 1977. 34(5): p. 518-522.
16. Edmonds, C.G., et al., Analysis of mutagens from cooked foods by directly combined liquid chromatography-mass spectrometry. *Environmental health perspectives*, 1986. 67: p. 35-40.
17. Jiang, T., et al., Capillary enzyme immunoassay with electrochemical detection for the determination of atrazine in water. *Journal of Agricultural and Food Chemistry*, 1995. 43(4): p. 1098-1104.
18. Moine, H., et al., The RNA binding site of S8 ribosomal protein of Escherichia coli: Selex and hydroxyl radical probing studies. *RNA*, 1997. 3(3): p. 255-268.
19. Bai, J., et al., Ultrasensitive sensing of diethylstilbestrol based on AuNPs/MWCNTs-CS composites coupling with sol-gel molecularly imprinted polymer as a recognition element of an electrochemical sensor. *Sensors and Actuators B: Chemical*, 2017. 238: p. 420-426.
20. Qaddare, S.H. and A. Salimi, Amplified fluorescent sensing of DNA using luminescent carbon dots and AuNPs/GO as a sensing platform: A novel coupling of FRET and DNA hybridization for homogeneous HIV-1 gene detection at

femtomolar level. *Biosensors and Bioelectronics*, 2017. 89: p. 773-780.

21. Mascini, M., et al., Hairpin DNA-AuNPs as molecular binding elements for the detection of volatile organic compounds. *Biosensors and Bioelectronics*, 2019. 123: p. 124-130.
22. Baetsen-Young, A.M., et al., Direct colorimetric detection of unamplified pathogen DNA by dextrin-capped gold nanoparticles. *Biosensors and Bioelectronics*, 2018. 101: p. 29-36.
23. De Luca, G., et al., Tripodal tris-disulfides as capping agents for a controlled mixed functionalization of gold nanoparticles. *New Journal of Chemistry*, 2018. 42(20): p. 16436-16440.
24. Wu, S., et al., Gold nanoparticles dissolution based colorimetric method for highly sensitive detection of organophosphate pesticides. *Sensors and Actuators B: Chemical*, 2017. 238: p. 427-433.
25. Chen, H., K. Zhou, and G. Zhao, Gold nanoparticles: From synthesis, properties to their potential application as colorimetric sensors in food safety screening. *Trends in Food Science & Technology*, 2018. 78: p. 83-94.
26. Memon, S.S., et al., Sensitive and selective aggregation based colorimetric sensing of Fe3+ via interaction with acetyl salicylic acid derived gold nanoparticles. *Sensors and Actuators B: Chemical*, 2018. 259: p. 1006-1012.
27. Mafuné, F., et al., Full physical preparation of size-selected gold nanoparticles in

solution: laser ablation and laser-induced size control. *The Journal of Physical Chemistry B*, 2002. 106(31): p. 7575-7577.

28. Ding, Y., et al., Gold nanoparticles for nucleic acid delivery. *Molecular therapy*, 2014. 22(6): p. 1075-1083.
29. Turkevich, J., P.C. Stevenson, and J. Hillier, A study of the nucleation and growth processes in the synthesis of colloidal gold. *Discussions of the Faraday Society*, 1951. 11: p. 55-75.
30. Frens, G., Controlled nucleation for the regulation of the particle size in monodisperse gold suspensions. *Nature physical science*, 1973. 241(105): p. 20-22.
31. Bastús, N.G., J. Comenge, and V. Puntes, Kinetically controlled seeded growth synthesis of citrate-stabilized gold nanoparticles of up to 200 nm: size focusing versus Ostwald ripening. *Langmuir*, 2011. 27(17): p. 11098.
32. Cheng, Y., et al., Highly efficient drug delivery with gold nanoparticle vectors for in vivo photodynamic therapy of cancer. *Journal of the American Chemical Society*, 2008. 130(32): p. 10643-10647.
33. Brust, M., et al., Synthesis of thiol-derivatised gold nanoparticles in a two-phase liquid–liquid system. *Journal of the Chemical Society, Chemical Communications*, 1994(7): p. 801-802.
34. Zhang, Y., et al., Colorimetric detection based on localised surface plasmon

resonance of gold nanoparticles: merits, inherent shortcomings and future prospects. *Talanta*, 2016. 152: p. 410-422.

35. Xia, N., et al., Visual and fluorescent assays for selective detection of beta-amyloid oligomers based on the inner filter effect of gold nanoparticles on the fluorescence of CdTe quantum dots. *Biosensors and Bioelectronics*, 2016. 85: p. 625-632.
36. Zhu, J., et al., Dual-mode melamine detection based on gold nanoparticles aggregation-induced fluorescence "turn-on" and "turn-off" of CdTe quantum dots. *Sensors and Actuators B: Chemical*, 2017. 239: p. 906-915.
37. Fang, C., et al., Gold nanoparticle-based optical sensors for selected anionic contaminants. *TrAC Trends in Analytical Chemistry*, 2017. 86: p. 143-154.
38. Jain, P.K., et al., Calculated absorption and scattering properties of gold nanoparticles of different size, shape, and composition: applications in biological imaging and biomedicine. *The journal of physical chemistry B*, 2006. 110(14): p. 7238-7248.
39. Njoki, P.N., et al., Size correlation of optical and spectroscopic properties for gold nanoparticles. *The Journal of Physical Chemistry C*, 2007. 111(40): p. 14664-14669.
40. Wang, Z. and L. Ma, Gold nanoparticle probes. *Coordination Chemistry Reviews*, 2009. 253(11-12): p. 1607-1618.

41. Tan, J., et al., Controllable aggregation and reversible pH sensitivity of AuNPs regulated by carboxymethyl cellulose. *Langmuir*, 2010. 26(3): p. 2093-2098.
42. Gestwicki, J.E., L.E. Strong, and L.L. Kiessling, Visualization of single multivalent receptor–ligand complexes by transmission electron microscopy. *Angewandte Chemie International Edition*, 2000. 39(24): p. 4567-4570.
43. Sardar, R., et al., Gold nanoparticles: past, present, and future. *Langmuir*, 2009. 25(24): p. 13840-13851.
44. Liu, Y., et al., Simple, rapid, homogeneous oligonucleotides colorimetric detection based on non-aggregated gold nanoparticles. *Chemical Communications*, 2012. 48(26): p. 3164-3166.
45. Bai, L.-Y., et al., Rapid, sensitive and selective detection of pymetrozine using gold nanoparticles as colourimetric probes. *Micro & Nano Letters*, 2010. 5(5): p. 304-308.
46. Tsogas, G.Z., et al., Recent advances in nanomaterial probes for optical biothiol sensing: a review. *Analytical Letters*, 2018. 51(4): p. 443-468.
47. Häkkinen, H., The gold–sulfur interface at the nanoscale. *Nature chemistry*, 2012. 4(6): p. 443.
48. Liu, D., Z. Wang, and X. Jiang, Gold nanoparticles for the colorimetric and fluorescent detection of ions and small organic molecules. *Nanoscale*, 2011. 3(4): p. 1421-1433.

49. Ding, N., et al., A simple colorimetric sensor based on anti-aggregation of gold nanoparticles for Hg^{2+} detection. *Colloids and Surfaces A: Physicochemical and Engineering Aspects*, 2012. 395: p. 161-167.
50. Chen, L., et al., A highly selective and sensitive colorimetric sensor for iodide detection based on anti-aggregation of gold nanoparticles. *Sensors and Actuators B: Chemical*, 2013. 182: p. 482-488.
51. Lu, L., J. Zhang, and X. Yang, Simple and selective colorimetric detection of hypochlorite based on anti-aggregation of gold nanoparticles. *Sensors and Actuators B: Chemical*, 2013. 184: p. 189-195.
52. Hormozi-Nezhad, M.R. and S. Abbasi-Moayed, A sensitive and selective colorimetric method for detection of copper ions based on anti-aggregation of unmodified gold nanoparticles. *Talanta*, 2014. 129: p. 227-232.
53. Chen, W., et al., Detection of the nanomolar level of total Cr [(III) and (VI)] by functionalized gold nanoparticles and a smartphone with the assistance of theoretical calculation models. *Nanoscale*, 2015. 7(5): p. 2042-2049.
54. Ma, X., et al., A novel aptasensor for the colorimetric detection of S. typhimurium based on gold nanoparticles. *International journal of food microbiology*, 2017. 245: p. 1-5.
55. Du, J., et al., Colorimetric detection of Listeria monocytogenes using one-pot biosynthesized flower-shaped gold nanoparticles. *Sensors and Actuators B:*

Chemical, 2018. 265: p. 285-292.

56. Su, H., et al., Gold nanoparticles as colorimetric sensor: A case study on E. coli O157: H7 as a model for Gram-negative bacteria. *Sensors and Actuators B: Chemical*, 2012. 161(1): p. 298-303.
57. Thiramanas, R. and R. Laocharoensuk, Competitive binding of polyethyleneimine-coated gold nanoparticles to enzymes and bacteria: a key mechanism for low-level colorimetric detection of gram-positive and gram-negative bacteria. *Microchimica Acta*, 2016. 183(1): p. 389-396.
58. Martinović, T., et al., Foodborne pathogens and their toxins. *Journal of Proteomics*, 2016. 147: p. 226-235.
59. Fletcher, S., et al., Investigating an outbreak of staphylococcal food poisoning among travellers across two Australian states. *Western Pacific surveillance and response journal: WPSAR*, 2015. 6(2): p. 17.
60. Binh, D.X., N.N. Minh, and D.T. Nguyet, Prevalence of Listeria monocytogenes, E. coli, Salmonella Spp. and Staphylococcus aureus bacteria contamination on meat at public market in the north of Vietnam. *SOJ Microbiology and Infectious Diseases*, 2017. 5: p. 1-22.
61. Adley, C.C., Past, present and future of sensors in food production. *Foods*, 2014. 3(3): p. 491-510.
62. Zhang, C. and J. Zhang, Current techniques for detecting and monitoring algal

toxins and causative harmful algal blooms. *J. Environ. Anal. Chem*, 2015. 2(123): p. 2380-2391.1000123.

63. Khan, S.A., et al., Rapid and sensitive detection of cholera toxin using gold nanoparticle-based simple colorimetric and dynamic light scattering assay. *Analytica chimica acta*, 2015. 892: p. 167-174.
64. Liu, B.-H., et al., Development of a monoclonal antibody against ochratoxin A and its application in enzyme-linked immunosorbent assay and gold nanoparticle immunochromatographic strip. *Analytical chemistry*, 2008. 80(18): p. 7029-7035.
65. Shim, W.-B., K.-Y. Kim, and D.-H. Chung, Development and validation of a gold nanoparticle immunochromatographic assay (ICG) for the detection of zearalenone. *Journal of agricultural and food chemistry*, 2009. 57(10): p. 4035-4041.
66. Wang, X., R. Niessner, and D. Knopp, Magnetic bead-based colorimetric immunoassay for aflatoxin B1 using gold nanoparticles. *Sensors*, 2014. 14(11): p. 21535-21548.
67. Zhu, Y., et al., G-quadruplex DNAzyme-based microcystin-LR (toxin) determination by a novel immunosensor. *Biosensors and Bioelectronics*, 2011. 26(11): p. 4393-4398.
68. Yang, C., et al., Aptamer-based colorimetric biosensing of Ochratoxin A using unmodified gold nanoparticles indicator. *Biosensors and Bioelectronics*, 2011.

26(5): p. 2724-2727.

69. Luan, Y., et al., Visual and microplate detection of aflatoxin B2 based on NaCl-induced aggregation of aptamer-modified gold nanoparticles. *Microchimica Acta*, 2015. 182(5-6): p. 995-1001.
70. Chen, X., et al., Method for the quantification of current use and persistent pesticides in cow milk, human milk and baby formula using gas chromatography tandem mass spectrometry. *Journal of Chromatography B*, 2014. 970: p. 121-130.
71. Darko, G. and S.O. Acquaah, Levels of organochlorine pesticides residues in meat. *International Journal of Environmental Science & Technology*, 2007. 4(4): p. 521-524.
72. Bakırcı, G.T., et al., Pesticide residues in fruits and vegetables from the Aegean region, Turkey. *Food chemistry*, 2014. 160: p. 379-392.
73. Tanaka, Y., et al., 15N− 15N J-coupling across HgII: direct observation of HgII-mediated T− T base pairs in a DNA duplex. *Journal of the American Chemical Society*, 2007. 129(2): p. 244-245.
74. Lee, J.S., M.S. Han, and C.A. Mirkin, Colorimetric detection of mercuric ion (Hg^{2+}) in aqueous media using DNA-functionalized gold nanoparticles. *Angewandte Chemie International Edition*, 2007. 46(22): p. 4093-4096.
75. Wang, Z., J.H. Lee, and Y. Lu, Label-free colorimetric detection of lead ions with a nanomolar detection limit and tunable dynamic range by using gold

nanoparticles and DNAzyme. *Advanced Materials*, 2008. 20(17): p. 3263-3267.

76. Guo, Y., et al., Colorimetric detection of mercury, lead and copper ions simultaneously using protein-functionalized gold nanoparticles. *Biosensors and Bioelectronics*, 2011. 26(10): p. 4064-4069.
77. Chu, W., et al., A biomimetic sensor for the detection of lead in water. *Biosensors and Bioelectronics*, 2015. 67: p. 621-624.
78. Bai, W., et al., Gold nanoparticle–based colorimetric aptasensor for rapid detection of six organophosphorous pesticides. *Environmental toxicology and chemistry*, 2015. 34(10): p. 2244-2249.
79. Bala, R., et al., Ultrasensitive aptamer biosensor for malathion detection based on cationic polymer and gold nanoparticles. *Biosensors and Bioelectronics*, 2016. 85: p. 445-449.
80. Kim, Y.-J., et al., New colorimetric aptasensor for rapid on-site detection of Campylobacter jejuni and Campylobacter coli in chicken carcass samples. *Analytica chimica acta*, 2018. 1029: p. 78-85.
81. Li, F., et al., Asymmetric polymerase chain assay combined with propidium monoazide treatment and unmodified gold nanoparticles for colorimetric detection of viable emetic Bacillus cereus in milk. *Sensors and Actuators B: Chemical*, 2018. 255: p. 1455-1461.
82. Schofield, C.L., R.A. Field, and D.A. Russell, Glyconanoparticles for the

colorimetric detection of cholera toxin. *Analytical chemistry*, 2007. 79(4): p. 1356-1361.

83. Uzawa, H., et al., A novel sugar-probe biosensor for the deadly plant proteinous toxin, ricin. *Biosensors and Bioelectronics*, 2008. 24(4): p. 923-927.
84. Xue, X., F. Wang, and X. Liu, One-step, room temperature, colorimetric detection of mercury (Hg^{2+}) using DNA/nanoparticle conjugates. *Journal of the American Chemical Society*, 2008. 130(11): p. 3244-3245.
85. Du, J., et al., Flexible colorimetric detection of mercuric ion by simply mixing nanoparticles and oligopeptides. *Small*, 2011. 7(10): p. 1407-1411.
86. Zhang, X., et al., Ionic liquid functionalized gold nanoparticles: Synthesis, rapid colorimetric detection of imidacloprid. *Sensors and Actuators B: Chemical*, 2014. 191: p. 313-319.
87. Kumar, N., et al., Colorimetric determination of melamine in milk using unmodified silver nanoparticles. *Spectrochimica Acta Part A: Molecular and Biomolecular Spectroscopy*, 2016. 156: p. 89-97.
88. Cai, H.-H., et al., Visual and absorption spectroscopic detections of melamine with 3-mercaptopriopionic acid-functionalized gold nanoparticles: A synergistic strategy induced nanoparticle aggregates. *Journal of Food Engineering*, 2014. 142: p. 163-169.
89. Wu, Z., et al., Colorimetric detection of melamine during the formation of gold

nanoparticles. *Biosensors and Bioelectronics*, 2011. 26(5): p. 2574-2578.

Chapter II. Visible on-site detection of Ara h 1 by the switchable-linker-mediated precipitation of gold nanoparticles

II -1. Introduction

Food allergies are a significant issue worldwide for both food industries and public health. Because no effective cure has been developed for food allergies, avoidance of foods containing allergen(s) is the most appropriate way to prevent reactions or problems [1]. For this reason, many countries have established regulations for labelling allergenic ingredients in pre-packaged foods [2, 3], and many food manufacturers voluntarily perform precautionary allergen labelling (PAL) [4-6]. However, these warnings are often ignored by consumers due to mislabelled PAL that are not based on a quantitative allergen risk assessment [7]. Therefore, it is essential to engage the public in the analysis of food allergens by developing consumer-friendly detection methods. Seventy-five percent of peanut-allergic individuals are reported to have serum-specific IgE against the peanut protein 7S globulin (Ara h 1), which accounts for 12–16% of peanut protein [8]. Ara h 1 is composed of a stable homo-trimer that is bound by hydrophobic interactions between residues in the α-helical bundles of 63.5 kDa monomers [9, 10]. Therefore, Ara h 1, which has a stable structure, is widely used as a representative allergen marker [11].

In recent decades, many effective techniques have been extensively

applied to ensure the proper labelling and management of food allergens, including Ara h 1. These techniques include the enzyme-linked immunosorbent assay (ELISA) [12, 13], reverse-phase high-performance chromatography (RP-HPLC) [14], surface enhanced Raman spectroscopy [15], magneto-resistive [16], electrochemical sensors [17], DNA-based sensors [18], real-time polymerase chain reaction (PCR) [19, 20] and the loop-mediated isothermal amplification (LAMP) [21]. Despite these many methods, a need remains for the development of on-site detection methods that can be used without time-consuming preparation, trained experts and/or sophisticated instruments.

In this paper, my aim was to provide a simple and fast method for the on-site detection of Ara h 1 as a model allergen target based on my developed gold nanoparticle (AuNP)-precipitation-based detection system [22-25]. This technique generates a visible signal with the precipitation of aggregates of AuNP and the target protein. A key element in determining the aggregate size is the switchable linker (SL), with the precipitation of aggregates generated by changing the ratio of AuNP to SL, thereby enabling quantitative detection of the target. This detection method includes a simple extraction process using an easy-to-use syringe filter and a AuNP precipitation analysis method

suitable for field use. To evaluate the practical detection limit and quantification of Ara h 1, the proposed analytical method is performed with reference to the analytical sensitivity threshold recommended by the Voluntary Incidental Trace Allergen Labelling (VITAL 3.0) system [26]. In addition, the developed method can evaluate selectivity based on excellent visible signals. Taken together, the results obtained by this proposed method demonstrate its practicality and simplicity in the detection of Ara h 1 in foods.

II-2. Materials and Methods

II-2.1. Materials

Chloroauric acid and bovine serum albumin (BSA) were purchased from Sigma Aldrich (St. Louis, MO, USA). Tri-sodium citrate was purchased from Yakuri Pure Chemicals Co., Ltd (Kyoto, Japan). Tetraborate pH standard solution was purchased from Wako Pure Chemicals Industries, Ltd (Osaka, Japan). Phosphate-buffered saline (PBS) was purchased from Thermo Fisher Scientific (Waltham, MA, USA). Thiolated streptavidin was purchased from Protein Mods (Madison, WI, USA). Purified natural Ara h 1, biotinylated monoclonal anti-Ara h 1 IgG1 (clone 2F7 C12 D10) antibody, and Ara h 1 ELISA kit EL-AH1, which contains mouse monoclonal IgG1 (2C12) and biotinylated mouse monoclonal IgG1 (2F7), were purchased from Indoor Biotechnologies (Cardiff, UK). The method used by the ELISA kit to detect Ara h 1 is included in the supplementary information. The filter (0.45-μm pore size) was purchased from Milipore (Billerica, MA, USA). Roasted peanuts, tree nuts (almonds, cashew nuts, hazelnuts, pecans, and walnuts), and legumes (black-eyed peas and soybeans) were purchased from Lotte, Ltd (Seoul, Korea). Skippy creamy peanut butter were purchased from Hormel Foods,

LLC (Austin, MN, USA).

II-2.2. Instrumentation

Absorbance measurements were performed on a UV-1700 spectrophotometer (Shimadzu, Kyoto, Japan). The pH values of all buffer solutions were determined using the Professional Meter PP-15 (Satorious, Göttingen, Germany). Particle sizes and distributions were determined by dynamic light scattering (DLS) with a Zetasizer Nano-ZS 90 (Malvern, Worcestershire, UK). Transmission electron microscopic (TEM) images were obtained using a LIBRA 120 transmission electron microscope (Karl Zeiss, Oberkochen, Germany).

II-2.3. Preparation of gold nanoparticles (AuNP)

Gold nanoparticles (AuNP) 30.0 ± 0.5 nm in diameter were synthesised according to the method established by Bastus et al. [27]. Briefly, 150 mL of sodium citrate solution (2.2 mM) was brought to boiling. Once boiling had begun, 1 mL of chloroauric acid ($HAuCl_4$) solution (25 mM) was added to the boiling solution. When the colour of the solution had changed to soft pink, the solution was cooled to 90 °C in a water bath, and the cooled

solution was used as a seed solution for the growth process. To grow the AuNP, 1 mL of $HAuCl_4$ solution (25 mM) was added to the seed solution twice at 30-min intervals. After the reaction was finished, 55 mL of the sample was extracted. The remaining sample was then diluted by adding 55 mL of a sodium citrate solution (2.2 mM). After the temperature of the diluted solution had returned to 90 °C, the growth process was repeated using the diluted solution as the seed solution. This process was repeated three times. Ultimately, AuNP 30 nm in diameter were obtained and stored at 4 °C until further use. The particle sizes of the AuNP were determined using an ultraviolet/visible (UV/Vis) spectrophotometer and DLS.

II-2.4. Preparation of streptavidin-coated gold nanoparticles (stAuNP)

Six hundred microliters of AuNP (absorbance of 4.0 at 526.0 ± 0.5 nm, diameter of 30 nm) were incubated with 100 µL of BSA (100 µg/mL) in borate buffer (pH 7.4) for 30 min. After incubation, the mixture was reacted with 100 µL of thiolated streptavidin (50 µg/mL) in borate buffer (pH 7.4) for 30 min. Unbound streptavidin was removed by repeated centrifugation (relative centrifugal force, 5000, 30 min), and pellets of streptavidin-coated AuNP (stAuNP) were resuspended in PBS 1× (pH 7.4) containing 0.05% (w/v) BSA. The concentration was then adjusted to an absorbance of 6.0 at 536.0 ± 0.5 nm

(Figure II-S1B). This concentration of AuNP in solution was estimated based on the absorbance value as $\sim 1.19\times10^{12}$ particles per mL. The additional physicochemical analysis of the surface modification of the AuNP used in this study is shown in Figure II-S1 and detailed in Table II-S1.

I controlled the degree of coating of streptavidin by first coating BSA on the AuNP and then coating streptavidin on the empty spaces remaining on the surfaces of the AuNP. The tetrameric structure of streptavidin can induce aggregation of AuNP, whereas the stable monomeric structure of BSA does not.

Table II-S1. Physicochemical characteristics of the surface-modified AuNP

Samples	Zeta potential (mV)	Diameter (nm)	PDI value[a]
AuNP	-34.43 ± 1.77	29.61 ± 0.31	0.202 ± 0.005
stAuNP	-9.35 ± 0.56	44.59 ± 0.94	0.257 ± 0.007

[a] PDI is the polydispersity index

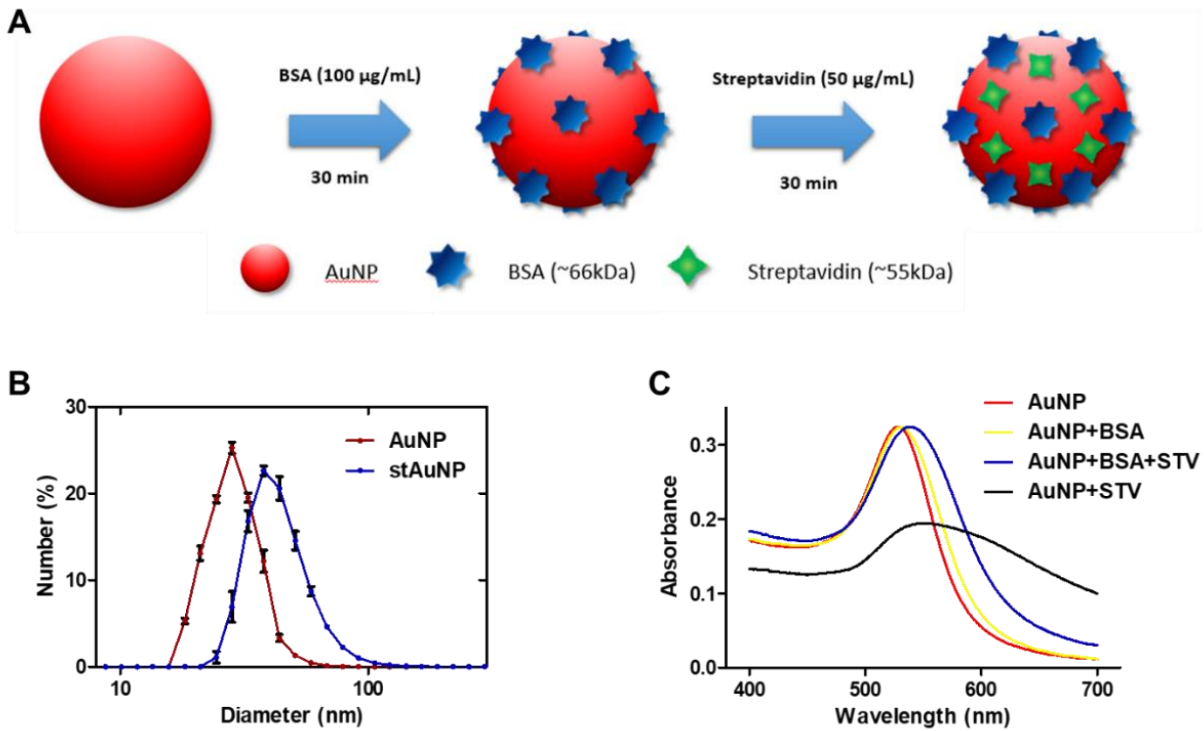

Figure II-S1. (A) Schematic of surface modification of AuNP. The analysis of AuNP physicochemical characteristics was performed by (B) dynamic light scattering (DLS) and (C) ultraviolet/visible (UV/Vis) spectroscopy.

II-2.5. Detection of Ara h 1 in standard solution

The detection system comprised two steps. In the first step, 100 µL of standard Ara h 1 solution (0, 25 ng/mL, 250 ng/mL, 2.5 µg/mL, 5.0 µg/mL and 10.0 µg/mL), which was a part of the purchased ELISA kit, was mixed with biotinylated anti-Ara h1 antibody (b-Ab) in concentrations ranging from 0.5 µg/mL to 0.9 µg/mL. The mixture was then mildly agitated for 15 min. In the second step, 200 µL of stAuNP (absorbance of 6.0 at 536.0 ± 0.5 nm) was added and then agitated for an additional 15 min. The shift in the range exhibiting a visible colour change, which is referred to as the REVC, was identified visually and/or by UV/Vis spectroscopy in the 400–700 nm range. A standard Ara h 1 solution was prepared by diluting purchased Ara h 1 in PBS 1× (pH 7.4).

II-2.6. Preparation of model cookies for a detection experiment on a real matrix

For use in a real-sample detection experiment, sample cookies were prepared using the following procedure. The cookie ingredients were purchased at a local market. Eighty grams of brown sugar (CJ CheilJedang,

Incheon, South Korea) and 0.5 g of salt (Taepyung Salt Co., Shinan, South Korea) were mixed into and dissolved in 80 g of melted butter (Lotte Food, Cheonan, South Korea). One egg (Tetgol Farm Co., Youngin, South Korea) and 1 g of pure vanilla extract (Lorannoils INC., MI, USA) were added and uniformly mixed into the blended butter solution to obtain a premix. Dry ingredients, including 150 g of wheat flour (CJ CheilJedang, Yangsan, South Korea) and 1 g of baking soda (Bread Garden, Seongnam, South Korea), were then combined with the premix. To produce a model cookie, roasted peanuts (Qingdao Jiaoping Foods Co., Qingdao, China) were ground into powder in a blade-mixer (SFM-500SP, Shin-Il, South Korea) and 0.0025 wt%, 0.025 wt%, 0.5 wt%, 1 wt%, and 5 wt% of powdered peanut were mixed into each premix. The fully homogenised dough was divided into 30-g portions for each sample to ensure that the cookies were of the same size. The cookies were baked in a light-wave oven (KAO-H013, KitchenArt, South Korea) for 20 min at 180 °C.

II-2.7. Detection of Ara h 1 in cookie extract solution

Sample extracts were prepared according to previously described procedures [28] with minor modifications. Briefly, 30 g of the sample was ground and dissolved into 300 mL of 20 mM Tris-HCl buffer (pH 8.5), which

was then agitated for 15 min at room temperature. The extracts were filtered through a 0.45-µm syringe filter to remove solid debris. The filtered cookie extract solutions were diluted 10-fold with PBS 1x (pH 7.4) and then mixed with b-Ab ranging in concentrations from 0.5 µg/mL to 0.9 µg/mL. The remaining steps were performed in the manner described above. The Ara h 1 concentration in the cookie extract solution was measured using the commercial ELISA kit.

II-2.8. Verification of the selectivity of the detection method

Cookie samples containing 5.0 wt% tree nuts (almond, cashew nut, hazelnut, pecan, and walnut) and legumes (soybean, and black-eyed pea) were used in the selectivity tests. Each sample extract solution was diluted 10-fold with PBS 1x (pH 7.4) and then mixed with b-Ab ranging in concentrations from 0.5 µg/mL, 0.7 µg/mL and 0.9 µg/mL. The remaining steps were performed in the manner described above.

II-2.9. Statistical analysis

The data represent an average of at least three independent

experiments or measurements, and the results are expressed as mean ± standard deviation (SD).

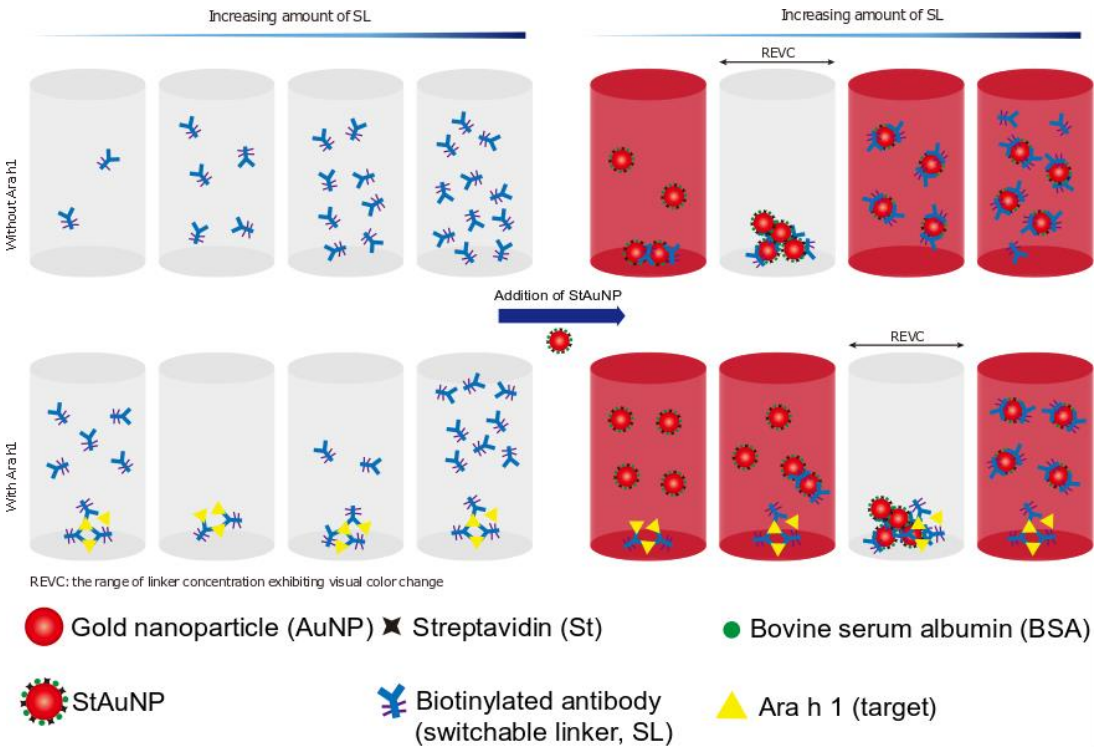

Figure II-1. Schematic of the colorimetric and visual detection of Ara h 1 based on the shift in the range of the exhibiting visible colour change (REVC).

II-3. Results and Discussion

II-3-1. Overall detection procedures

In this study, I focused on a detection process that could be used when on-site detection was required. I propose an easy and quick detection procedure that involves simple extraction and minimal pretreatment. Figure **II-**2 shows a schematic of the on-site detection procedure for Ara h 1 as a representative food allergen. This procedure enables Ara h 1 to be quickly, accurately, and sensitively detected in a real cookie using a simple device. First, the prepared model cookie can be easily crushed by hand and powdered for extraction. To realize short and simple extraction, the procedure is designed to perform extractions within 15 min at room temperature using Tris-HCl buffer (pH 8.5). The procedure consists of dissolution and purification steps. First, the crushed cookie is dissolved in Tris-HCl buffer for approximately 15 min, and then the extract is filtered through a readily available commercial 50-mL syringe and syringe filter (pore size 0.45 μm) to remove solid debris. Using this procedure, Ara h 1 can be extracted quickly and simply from cookies in the field. After simple extraction, the solution containing the target Ara h 1 is easily tested by the proposed detection system

based on SL-induced AuNP precipitation. This method is also designed specifically for field applications and requires no washing or complicated probe immobilisation procedures. In addition, the detection results can be visually read by the naked eye. To apply this procedure in the field problems such as automation, simplification, and miniaturisation of sample preparation and detection must be addressed, but the proposed detection procedure is considered to be a significant step toward on-site applications.

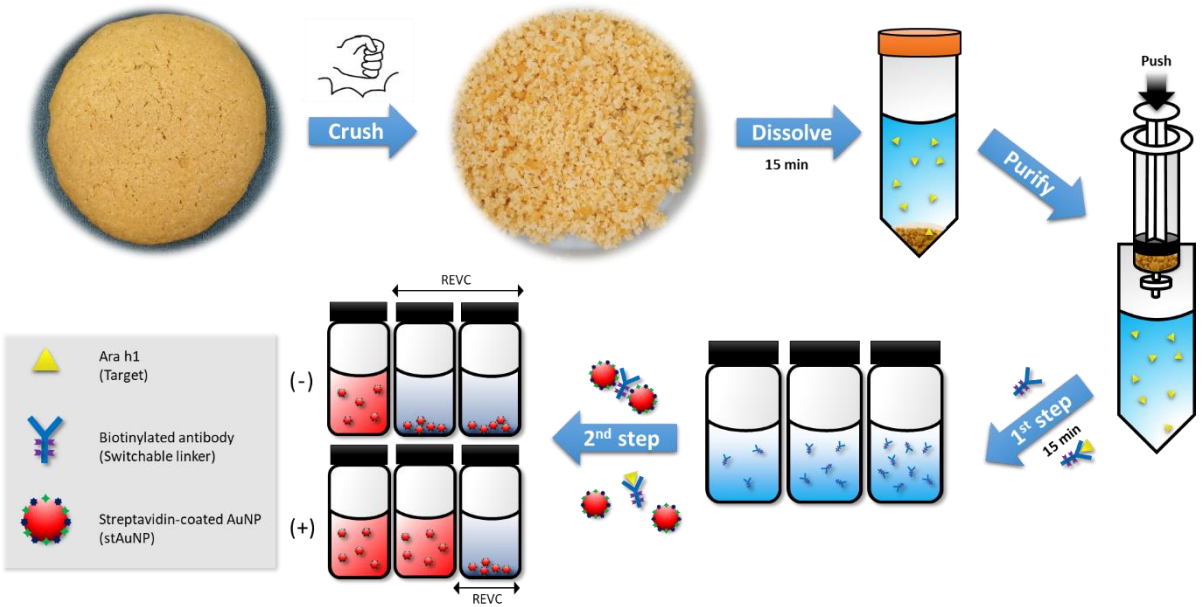

Figure II-2. Schematic of overall detection procedures, including peanut extraction and Ara h 1 detection.

II-3.2. Hypothesised mechanism for Ara h 1 detection

As shown in Figure **II-**1, the proposed method consists of a control line without a target and a test line with a target, and is designed to involve two sequential steps: (1) reaction of the SL (b-Ab) and the target (Ara h 1), i.e., the target recognition step, and (2) after the reaction time has elapsed, the addition of functionalised AuNP (stAuNP), i.e., the signal indication step. Two regions can be distinguished in the AuNP/SL aggregates: the REVC with colour change and the region with no colour change (in which the number of linkers that could react with the particles was insufficient or the binding site of the particles were already filled by the linker). The REVC of the control line was determined by the quantitative relationship between the AuNP and SL. In the test line with the target, the SL can be switched off as the SL binds to Ara h 1, which shifts the REVC to a higher linker concentration range than that of the control line. This colour difference can be used to quantitatively detect the target.

The hypothesised detection mechanism is shown in Figure II-1, which is based on the change in the aggregation pattern according to the quantitative correlations among the SL, targets, and AuNP. The SL is an aggregation mediator that can form aggregates with both the targets and AuNP. When the

AuNP and SL react at a specific ratio, they form large aggregates, which causes fast precipitation. However, if the target in the sample is preferentially recognised, an SL/target aggregate can form. The resulting aggregate interferes with the formation of AuNP and SL aggregates, which leads to a change in the optimum AuNP/SL ratio for rapid precipitation. Alteration in the precipitation rate of the AuNP/SL aggregates provokes a shift in the visible colour change (REVC) and absorbance in the solution containing them.

The SL used in this study was a crosslinking agent that recognises targets in addition to inducing the large-scale aggregation (aggregates can be precipitated) of AuNP. The SL can induce large-scale aggregations when a specific concentration ratio with AuNP is realized. In addition, when the SL is switched off by a specific target such as Ara h 1, this specific concentration ratio is readjusted to change the extent of the large-scale aggregation. Unlike colour changes, such as the red and/or blue shift in other colorimetric assays, the colorimetric signal generated by the precipitation of aggregates is more intuitive because the large-scale aggregation reduces the dispersion of AuNP in the system, such that the colour disappears.

The two-step reaction of this system clearly shows the difference in susceptibility between the Ara h 1-antibody interaction in the signal indication

step and the streptavidin-biotin binding in the target recognition step. In the Ara h 1–antibody and streptavidin–biotin cases, the equilibrium dissociation constants (K_d) are known to be roughly 10^{-12} M^{-1} and 10^{-15} M^{-1}, respectively [29, 30]. However, the difference in the dynamics of these two reactions do not affect the operation of the system, which can be readily explained. First, the system consists of two independent sequential steps (the Ara h 1–antibody interaction in the target recognition step and the streptavidin–biotin binding in the signal indication steps). Second, each reaction occurs at a different binding site and has a minimal effect on the other reaction. The reactions are not competitive. Third, the streptavidin/biotin reaction occurs much more rapidly than the Ara h 1/antibody reaction, which results in the rapid formation of large-scale aggregates of AuNP with the SL. These large-scale aggregates then precipitate by gravity depending on their size, which results in a visual signal. In this situation, even if the SL is switched on by the reverse reaction of Ara h 1/Ab (such as the SL being detached from the Ara h 1), it has little chance of reacting with the aggregates. This process occurs because the larger are the aggregates, the relatively slower is the reaction rate. Gold nanoparticles that do not participate in the formation of aggregates can bind with the switched-on SL, but this process would generate only relatively small-scale aggregates that cannot be precipitated and would be very unlikely to affect the REVC.

For these reasons, I believe that the reversibility issue has minimal impact on the sensitivity. In addition, there are some samples for which precipitation occurs slowly depending on the size of the aggregates after the detection time I set (30 min), but this is unrelated to the reversibility.

II-3.3. Detection of Ara h 1 in PBS using the proposed method

Before on-site application, this detection strategy must be optimised in terms of the Ara h 1-induced REVC shift that is influenced by the concentrations/ratios of b-Ab and stAuNP. To do so, first, I determined the REVC signal of the control (no target), as shown in Figure II-S2. This REVC signal was observed at b-Ab concentrations ranging from 0.5 μg/mL to 5.0 μg/mL. A clear precipitate among the stAuNP and b-Ab was observed at b-Ab concentrations ranging from 1.0 μg/mL to 2.0 μg/mL, whereas only a slight colour difference (purplish red) was observed at concentrations of 0.5 μg/mL (low end) and 3.0 μg/mL (high end). This colour difference can be mainly attributed to the surface plasmon resonance (SPR) difference due to the presence of small stAuNP-b-Ab aggregates that had not yet precipitated. In the treatment of Ara h 1 (10.0 μg/mL and 20.0 μg/mL in Figure II-S2), a right-side REVC shift, as compared with the control REVC, was observed in the b-

Ab concentration ranges of 1.0–4.0 μg/mL and 1.0–5.0 μg/mL, respectively. Then, I further subdivided the b-Ab concentration ranges used for the Ara h 1 detection to obtain a finer and more sensitive quantitative signal change (for example, the REVC shift), from which I determined the b-Ab concentration range to be 0.5–0.9 μg/mL (Ara h 1, 2.5–10.0 μg/mL). As shown in Figure II-3A, the REVC shift at the low end was clearly observed as the concentration of Ara h 1 was increased from 0 (control samples) to 10.0 μg/mL. When only b-Ab and stAuNP formed aggregates without Ara h 1 in the control samples, precipitation occurred at all concentrations, excepting the lowest b-Ab concentration of 0.5 μg/mL (the lowest in this experiment). However, the reaction of b-Ab with 2.5 μg of Ara h 1 showed no precipitation even at a concentration of 0.6 μg/mL (REVC shift occurred). As the amount of reacted Ara h 1 increased, the precipitation area (REVC) gradually shifted to higher SL concentrations. As shown in Figure II-3B and 3C, I identified the pattern of aggregate formation based on the presence or absence of Ara h 1 observed by TEM at 0.9 μg/mL of b-Ab. In the absence of Ara h 1, a large cluster several micrometers in size formed. In the presence of Ara h 1, however, aggregates among b-Ab, Ara h 1, and stAuNP were observed because they were not large enough to precipitate. It was easy to distinguish the precipitation area using the naked eye alone without the aid of an instrument.

To evaluate this strategy at the above SL concentrations, I used the ELISA method to detect and compare various concentrations of Ara h 1 (0, 2.5 μg/mL, 5.0 μg/mL, and 10.0 μg/mL) (Figure II-3A). With respect to the detection limit, using the proposed strategy and ELISA, I was able to detect Ara h 1 at the concentration of 250 ng/mL and 25.0 ng/mL, respectively (provided from Indoor Biotechnologies Inc.). In practice, the detection limit of the proposed method was more sensitive than that of the ELISA method, and the visual signal based on the REVC shift was easier to quantitatively confirm by the proposed method, as the ELISA method shows a colour change based on the colour density. In addition, the detection limit (25.0 ng) with enhanced visibility is considered to be meaningful because, to date, 0.19 mg of peanut protein has been generally required to induce an allergic reaction even in allergen-sensitised patients (Bureau, 2019). For these reasons, the proposed method is considered to be effective and practical for field applications.

According to the research of Remington et al. [31], the eliciting doses (ED) for an allergic reaction in 1% and 5% of the population, known as ED01 and ED05, are estimated to be 0.2 mg and 2.0 mg of protein for peanuts, respectively. In addition, to confirm the sensitivity of the SL-based assay in a purified buffer at the ED01 and ED05 levels (0.19 mg of peanut protein or

25.0 ng of Ara h 1 and 1.9 mg of peanut protein or 250 ng of Ara h 1), biotinylated antibody concentrations were further subdivided into 0.600 μg/mL, 0.625 μg/mL, 0.650 μg/mL, 0.675 μg/mL, and 0.700 μg/mL. As shown in Figure II-3D, as the concentration of Ara h 1 increased, the REVC shifted to a higher linker concentration.

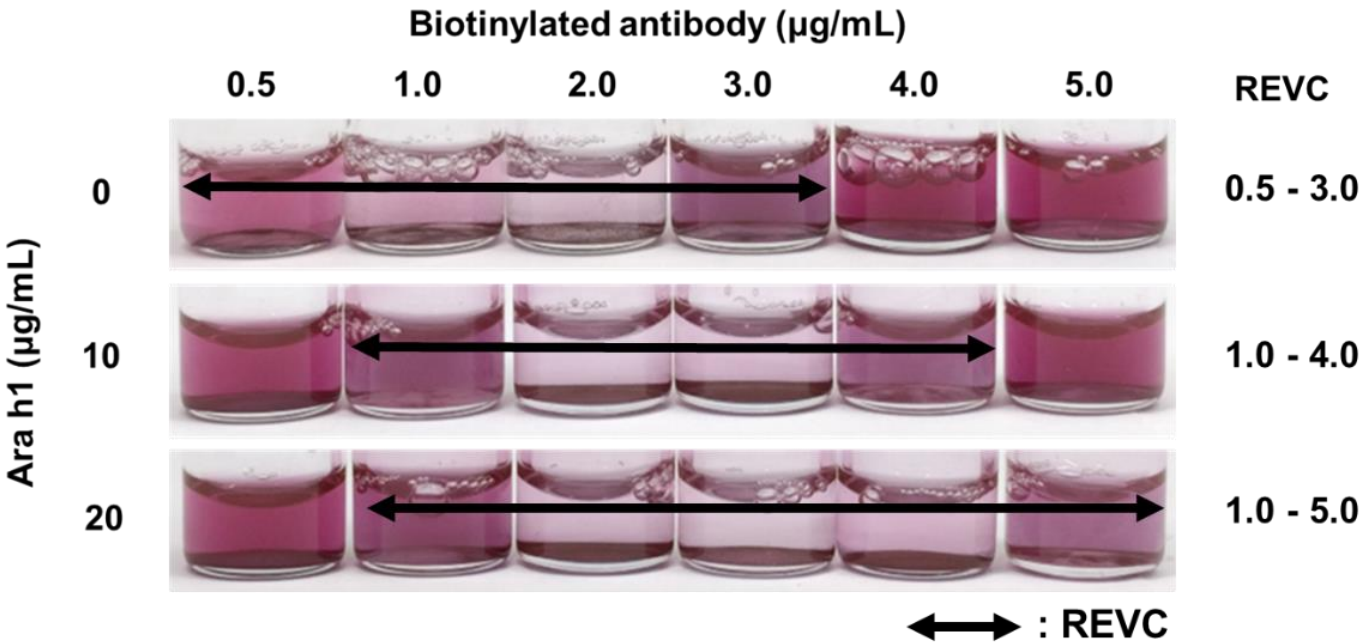

Figure II-S2. Shifting of the REVC in response to the presence of Ara h 1 in standard solution (0, 10 µg/mL and 20 µg/mL).

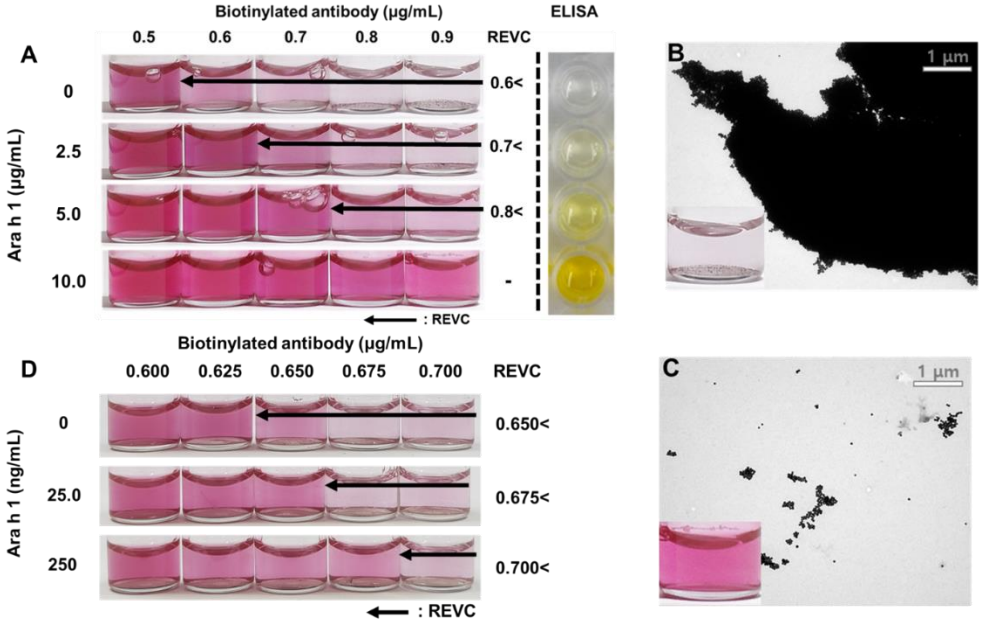

Figure II-3. (A) Detection of Ara h 1 (0.0, 2.5 μg/mL, 5.0 μg/mL, and 10.0 μg/mL) using the proposed switchable linker (SL)-based assay and the enzyme-linked immunosorbent assay (ELISA). Transmission electron micrographs of the Ara h 1-induced stAuNP aggregates (B, 0 μg/mL; C, 10.0 μg/mL) at 0.9 μg/mL of b-Ab (inset, photograph of their suspensions). (D) Detection of Ara h 1 (25.0 ng/mL and 250 ng/mL) using the proposed SL-based assay.

II-3.4. UV-Vis spectroscopic approach to Ara h 1 detection

To quantify the visual signal and improve the detection limit of the proposed method, I used a spectrophotometer to analyse the change in absorbance of AuNP aggregates based on the previously mentioned mechanism. The ratio between the AuNP and SL was optimised by testing various concentrations, and finally I identified 0.7 μg/mL of SL, which is a low-end concentration of the control line in Figure II-3A, for use in the experiment. As shown in Figure II-3A, as the concentration of Ara h 1 was increased at a linker concentration of 0.7 μg/mL, the colour change was confirmed as being due to the precipitation of gold aggregates. To confirm the correlation between the colour change and the concentration of Ara h 1, the change in absorbance was measured. Several Ara h 1 solutions with concentrations between 0.125 μg/mL and 20.0 μg/mL (Figure II-S3A) were tested. The changes in absorbance at a peak were found to be significant even with these small amounts of Ara h 1. I plotted the absorbance at 550 nm with the concentration of Ara h 1 to quantify the change in absorbance (Figure II-S3B). The absorbances at 550 nm were found to be proportional to the concentrations of Ara h 1 in the range from 0.125 μg/mL to 4.00 μg/mL, which can be expressed as a linear equation:

$$A_{550\ nm} = 0.0826C_{Ara\ h\ 1} + 0.1296\ (\mu g/mL) \quad (1)$$

with a correlation coefficient of 0.9982 at $A_{550\ nm}$ for absorbance at 550 nm and $C_{Ara\ h\ 1}$ for the concentration of Ara h 1. The linear section (detection range) occurred from 0.125 μg/mL to 4.00 μg/mL, and the slope of the absorbance change decreased at higher concentrations (from 4.00 μg/mL to 20.0 μg/mL). Unlike the change in absorbance, almost no shift was observed in the SPR peak (about 2 nm shift) of the small molecule–target AuNP aggregation. Thus, little change in colour was observed. This finding is thought to be the result of interference by proteins of the plasmon interactions with AuNP, because proteins are relatively larger than AuNP [32]. On the other hand, the speed and size of the AuNP/SL cluster formation were faster and larger than in the conventional AuNP aggregation-based detection method because of the number of biotin and streptavidin moieties, which can induce their aggregation on SL and stAuNP surfaces. Therefore, precipitation of the aggregates occurred within a short time (30 min), and the change in absorbance caused by this precipitation could be measured by a spectrophotometer.

Because AuNP induce colorimetric effects according to the localised surface plasmon resonance (LSPR) principle, nanoparticles in many studies have undergone changes in their size, shape, composition, and interparticle distance [33, 34]. The interparticle distance of AuNP in this system was especially important for inducing the LSPR of AuNP. The AuNP (30 ± 0.5 nm) used in this system were coated with BSA (66.5 kDa, 5.45-nm hydrodynamics radius) and streptavidin (52.8 kDa, 4.9-nm hydrodynamic radius), and these coated AuNP (stAuNP) were designed to crosslink with each other via the SL (IgG1, 11.5-nm hydrodynamic radius) [35, 36]. Therefore, even if stAuNP-b-Ab aggregates had caused LSPR, the distance between the particles was relatively large, so no dramatic colour changes (red to blue) occurred. In conclusion, when small stAuNP/b-Ab aggregates were formed, their weak colour changes via SPR could have occurred with a small peak shift (2 nm), as shown in Figure II-S3A.

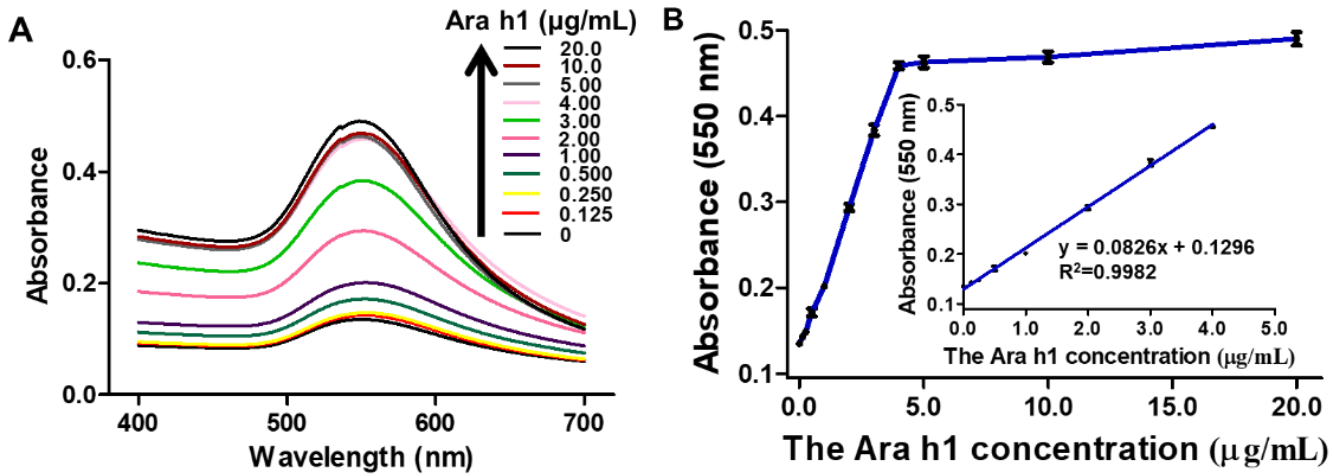

Figure II-S3. Ultraviolet/visible (UV/Vis) spectroscopy analysis. (A) Absorptive spectrum change in the proposed SL-based assay for the detection of Ara h 1 (0.125 μg/mL to 20.0 μg/mL) and (B) a plot of the absorbance at 550 nm versus the Ara h 1 concentration (inset, magnified linear region). All analyses were conducted on samples with an SL concentration of 0.7 μg/mL.

II-3.5. Selectivity of the detection method

To determine the selectivity of the SL-based colorimetric detection system with respect to Ara h 1, I used the proposed method to test control samples (only PBS), peanut extracts, and seven other samples, including five tree nuts (almond, cashew nut, hazelnut, pecan, and walnut) and two legumes (black-eyed pea and soybean). To make the SL-based detection system more field-applicable and to identify the potential risk of this system of being inhibited by the potential factors of real foods, I conducted a selectivity experiment using real foods containing different allergen proteins. As shown in Figure II-4, the REVC of the peanut extract shifted and no precipitation occurred in the selected linker concentrations (from 0.5 μg/mL to 0.9 μg/mL). However, all the other extracts exhibited an REVC similar to that of the control sample. In addition, as shown in Figure II-4B, if I compare the absorbance of each sample at a 0.7-μg/mL linker concentration, the significant difference in the visual effect of the peanut test group compared to the other test groups is confirmed. The real food groups used in this experiment consisted of various components, including fat, protein, and minerals in addition to a pigment that could inhibit the colorimetric reaction of the AuNP. Therefore, good selectivity in the detection of targets in real foods is critical for detection strategies. Based on the results of this experiment, I confirm that the REVC of a system can be

disturbed by the colour of the food itself in various food groups, including an almond, a cashew nut, or a black-eyed pea. However, having good selectivity with Ara h 1, this strategy clearly exhibits a colorimetric effect as an REVC if the appropriate linker concentrations (for example, 0.5 μg/mL and 0.9 ug/mL) are selected. Therefore, these results demonstrate that the proposed method has good selectivity and can be used for selective detection in mixed food samples.

It is very important to have good selectivity in the detection of a protein target in the extract of allergen-induced seed foods, because the extract contains a large number of soluble proteins, including 2S albumins [37], 7S globulins (vicilins) [38], and 11S globulins (legumins) [39, 40]. In addition, as no series of pretreatment steps is performed, such as a washing process, this detection process by extraction requires good selectivity from a large number of proteins that may be similar to the target. Based on this experiment, the proposed method not only demonstrated that it can operate selectively for a variety of similar proteins but also confirmed that Ara h 1 can be detected via a simple extraction method. As such, this strategy is considered to be very effective for field applications.

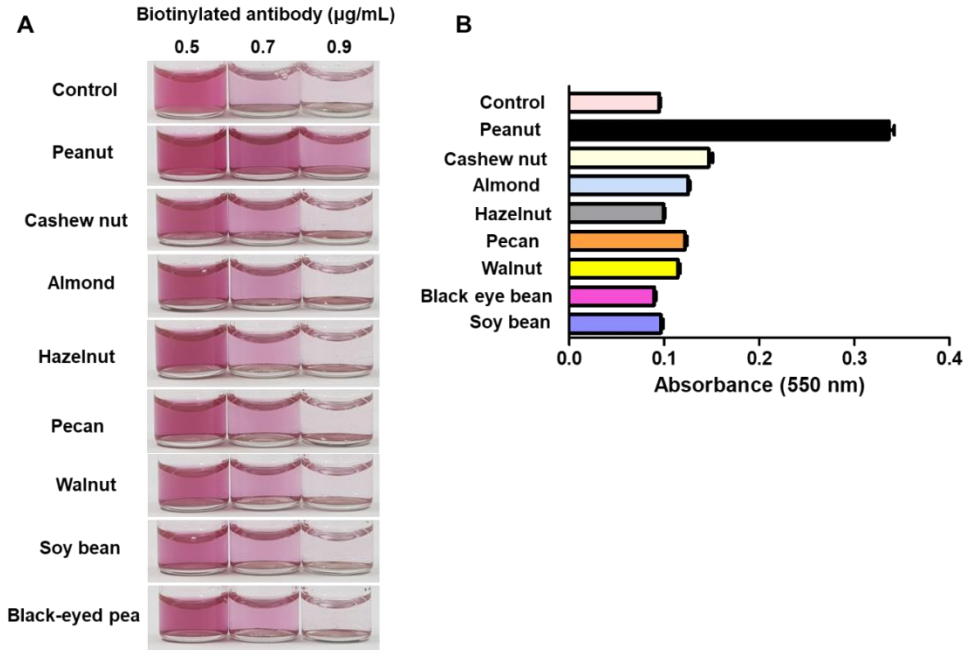

Figure II-4. Selectivity of the proposed SL-based colorimetric detection system. (A) The low-end REVC for detection with the solutions extracted from peanuts and several tree nuts (cashew nut, almond, hazelnut, pecan, and walnut) and legumes (soybean and black-eyed pea) (all extract solutions were diluted 10-fold with Tris-HCl buffer). (B) Comparison of absorbance at 550 nm of each sample with a biotinylated antibody concentration of 0.7 μg/mL. Control was a non-extract solution with Tris-HCl buffer.

II-3.6. Detection of Ara h 1 in model cookies

In this study, model cookies were prepared based on a one-piece serving (30 g), as established by the Food and Drug Administration (FDA) for the serving size of cookies. According to the VITAL® 3.0 reference dose, doses of 0.2 mg and 2.0 mg of peanut protein can trigger allergic reactions in 1% and 5% of the peanut-allergic population (ED01 and ED05), respectively. As peanuts have a conversion factor of four to allergenic food, less than 0.8 mg of peanuts can safely be included in food (Holzhauser et al., 2020). To determine the amounts of allowable peanut protein that satisfy the ED01 and ED05 safety criteria, cookies were made by mixing 0.75 mg and 7.5 mg of powdered peanut into each 30 g premix. These cookies had peanut protein contents equivalent to 0.19 mg and 1.9 mg, respectively, and 25.0 ng and 250 ng of Ara h 1 were detected in these same cookies. This amount of Ara h 1 corresponds to approximately 13.3% of total peanut protein, which is consistent with the previous study in which Ara h 1 accounts for 12–16% of the total peanut protein (Goliáš, Humlová, Halada, Hábová, Janatková, & Tučková, 2013). To evaluate the applicability of the proposed detection method to real samples, I detected estimated peanut-protein levels of 0.19 mg and 1.9 mg per 30 g of cookie (Figure-II-5B) and 38 mg, 75 mg, and 750 mg per 30 g of cookie (Figure II-5A). As shown in Figure II-5A, the detection

results exhibit a concentration-dependent shift in REVC. In the samples containing no peanut protein (control lines), precipitation as a visible signal occurred in the SL at concentrations above 0.5 μg/mL. As the concentration of peanut protein increased, the REVC shifted to higher SL concentration regions. As shown in Figure **II-**5B, I further subdivided the low-end region of the REVC, to determine the detection limit. The results showed a shift in the REVC down to a sample concentration of 0.19 mg of peanut protein per 30 g of cookie. These results indicate that the SL-based colorimetric detection method can detect peanut protein within 45 min to a concentration as low as 0.19 mg of peanut protein per 30 g of cookie, which satisfies ED01, and it exhibits the colorimetric effect (REVC shift) well without any inhibition even in real food. In addition, this result is significant in that the proposed detection process enables simple and fast field extraction of peanut protein and provides sensitive and convenient detection.

To validate the performance of my detection method, I compared my results with those obtained using a commercial ELISA method. Table II-1 summarises the experimental results I obtained for an Ara h 1 standard solution spiked with 10 mg/mL of Ara h 1 and food samples including roasted peanut extract and peanut butter extract. The recovery rates were 95.9%, 99.1%, and 106.6% of roasted peanut extract, peanut butter extract,

and Ara h 1 standard solution, respectively. A t-test was also performed and the calculated concentrations obtained using the SL-based colorimetric detection method were not statistically different from those obtained using the ELISA method, with a 95% of confidence interval. These results strongly indicate that the proposed method can be applied to determine the presence of peanut protein in real samples. Furthermore, to evaluate the performance of the proposed detection method, Table II-S2 presents a comparison of my proposed method with other published methods for Ara h 1 detection. The SL-based assay was confirmed to show good sensitivity in the detection of peanut protein in real food samples without the use of any special device.

Table II-1. Comparison of Ara h 1 detection in food samples using the enzyme-linked immunosorbent assay (ELISA) and the proposed method

Samples	Concentration of Ara h 1(mg/mL)[a]		Recovery (%)
	ELISA method	Developed method	
Roasted peanut extract	3.43 ± 0.18	3.29 ± 0.28	95.9
Peanut butter extract	4.63 ± 0.31	4.59 ± 0.43	99.1
Ara h 1 standard solution	10.00 ± 0.32	10.66 ± 0.36	106.6

[a] Data are mean values of triplicate measurements. Values are shown as means ± standard deviation.

Table II-S2. Comparison of the developed method in this work with other published detection methods for the detection of Ara h 1.

Method	Limit of detection	Detection time	Instrument	Sample type	Refs.
Surface enhanced Raman spectroscopy	0.14 mg/mL	Immediately	Raman spectroscope	Ara h 1 solution	[15]
Giant magnetoresistive sensor array	7.0 ng/mL	3.5 h	Magnetic field sensor	Ara h 1 solution	[16]
SWCNT-based biosensor	246.5 ng/mL	30 min	Gold microelectrode	Peanut butter, peanut chocolate, etc.	[17]
Loop-mediated isothermal amplification DNA biosensor	1 pg/mL (peanut DNA)	2.5 h	Heating block (PCR) Electrophoresis (spectrometry)	Boiled and steamed peanuts	[21]
Lateral flow assay	1 μg/mL	30 min	Not used	Raw peanut	[41]
Colorimetric biosensor	25.0 ng/mL	30 min	Not used	Peanut-containing sample (cookie)	This work

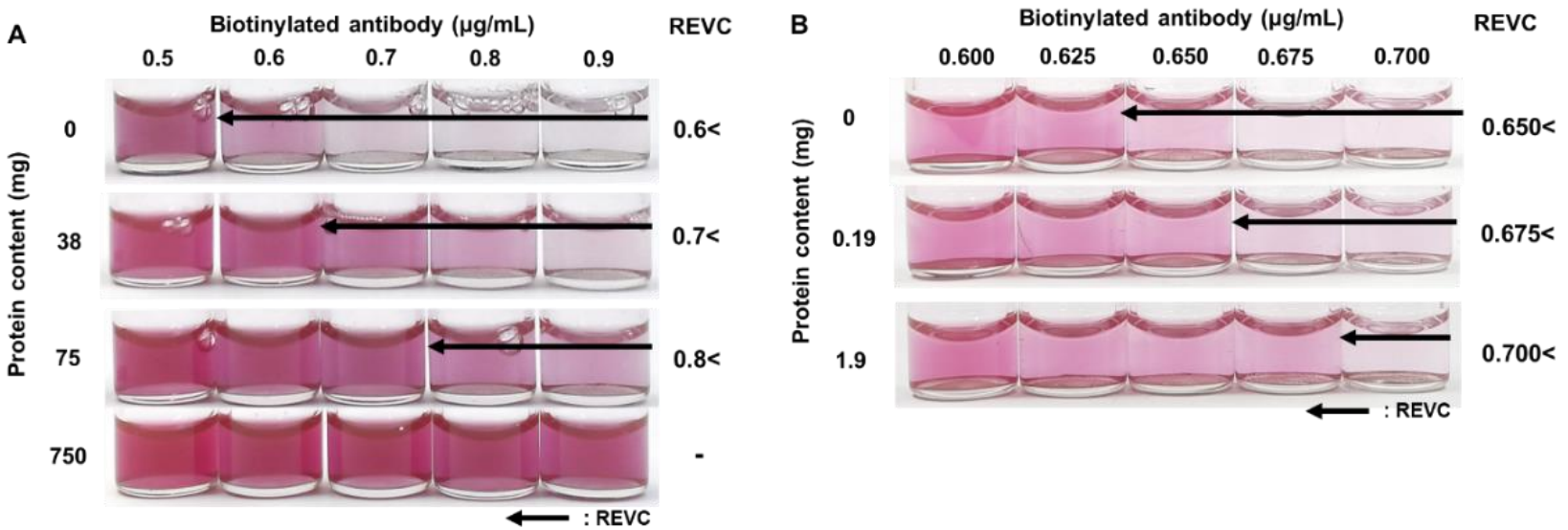

Figure II-5. Shift in the low-end REVC in response to the presence of Ara h 1 in cookie extract with 38 mg,75 mg, and 750 mg peanut protein (A) and 0.19 mg and 1.9 mg peanut protein (B) per 30 g of cookie.

II-4. Conclusions

Anaphylaxis induced by food allergens is a major issue in many countries, including the US, as no clear method has been developed for treating food allergies. As such, there are active and ongoing studies to monitor the food allergens present in various foods in the field. In this study, I proposed a simple method for extracting Ara h 1 from food through a syringe and a simple and rapid method for detecting Ara h 1 based on SL-induced AuNP precipitation. The detection results indicate that aggregates composed of AuNP and SL at specific concentration ratios undergo rapid precipitation, and Ara h 1 can interfere with this aggregation, thus causing a change in the concentration ratio at which precipitation occurs. Within 45 min, I was able to determine Ara h 1 concentrations as low as 25.0 ng/mL with the naked eye. In addition, when measured by a UV/Vis spectrophotometer, I observed a linear absorbance change in the concentration range of 125–4,000 ng/mL. This detection method also worked well using a cookie extract of a real food matrix, showing a good detection limit (0.19 mg of peanut protein per 30 g of cookie) and good selectivity. Although problems such as the simplification and automation of detection must be solved for field applications, SL-based assays provide visibility of results, time efficiency, and ease-of-use that are suitable in the field while also representing a promising alternative for the detection of other allergens.

II-5. References

1. Du Toit, G., et al., Food allergy: Update on prevention and tolerance. *Journal of Allergy and Clinical Immunology*, 2018. 141(1): p. 30-40.
2. Rizzi, C., et al., The Food Allergy Risk Management in the EU Labelling Legislation. *Journal of Agricultural and Environmental Ethics*, 2017. 30(2): p. 275-285.
3. Shoji, M., R. Adachi, and H. Akiyama, Japanese food allergen labeling regulation: an update. *Journal of AOAC International*, 2018. 101(1): p. 8-13.
4. Allen, K.J., et al., Precautionary labelling of foods for allergen content: are we ready for a global framework? *World Allergy Organization Journal*, 2014. 7(1): p. 1-14.
5. Crotty, M.P. and S.L. Taylor, Risks associated with foods having advisory milk labeling. *Journal of Allergy and Clinical Immunology*, 2010. 125(4): p. 935-937.
6. Remington, B., et al., Unintended allergens in precautionary labelled and unlabelled products pose significant risks to UK allergic consumers. *Allergy*, 2015. 70(7): p. 813-819.
7. Zhang, J., et al., Simultaneous determination of major peanut allergens Ara h1 and Ara h2 in baked foodstuffs based on their signature peptides using ultra-performance liquid chromatography coupled to tandem mass spectrometry. *Analytical Methods*, 2019. 11(12): p. 1689-1696.
8. Goliáš, J., et al., Identification of rice proteins recognized by the IgE antibodies of patients with food allergies. *Journal of agricultural and food chemistry*, 2013. 61(37): p. 8851-8860.
9. Burks, A.W., et al., Recombinant peanut allergen Ara h I expression and IgE binding in patients with peanut hypersensitivity. *The Journal of clinical investigation*, 1995. 96(4):

p. 1715-1721.

10. Van Boxtel, E.L., et al., Allergen Ara h 1 occurs in peanuts as a large oligomer rather than as a trimer. *Journal of agricultural and food chemistry*, 2006. 54(19): p. 7180-7186.

11. Palladino, C. and H. Breiteneder, Peanut allergens. *Molecular immunology*, 2018. 100: p. 58-70.

12. Jayasena, S., et al., Comparison of recovery and immunochemical detection of peanut proteins from differentially roasted peanut flour using ELISA. *Food chemistry*, 2019. 292: p. 32-38.

13. Montserrat, M., et al., Detection of peanut (Arachis hypogaea) allergens in processed foods by immunoassay: Influence of selected target protein and ELISA format applied. *Food control*, 2015. 54: p. 300-307.

14. Singh, H., et al., Standardization of RP-HPLC methods for the detection of the major peanut allergens Ara h 1, Ara h 2 and Ara h 3. *Food chemistry*, 2016. 194: p. 383-390.

15. Gezer, P.G., G.L. Liu, and J.L. Kokini, Development of a biodegradable sensor platform from gold coated zein nanophotonic films to detect peanut allergen, Ara h1, using surface enhanced raman spectroscopy. *Talanta*, 2016. 150: p. 224-232.

16. Ng, E., K.C. Nadeau, and S.X. Wang, Giant magnetoresistive sensor array for sensitive and specific multiplexed food allergen detection. *Biosensors and Bioelectronics*, 2016. 80: p. 359-365.

17. Sobhan, A., et al., Assessment of peanut allergen Ara h1 in processed foods using a SWCNTs-based nanobiosensor. *Bioscience, Biotechnology, and Biochemistry*, 2018. 82(7): p. 1134-1142.

18. Zhang, M., et al., Advanced DNA-based methods for the detection of peanut allergens

in processed food. *TrAC Trends in Analytical Chemistry*, 2019. 114: p. 278-292.

19. Miyazaki, A., et al., Real-time PCR detection methods for food allergens (wheat, buckwheat, and peanuts) using reference plasmids. *Journal of agricultural and food chemistry*, 2019. 67(19): p. 5680-5686.

20. Puente-Lelievre, C. and A.C. Eischeid, Development and evaluation of a real-time PCR multiplex assay for the detection of allergenic peanut using chloroplast DNA markers. *Journal of agricultural and food chemistry*, 2018. 66(32): p. 8623-8629.

21. Sheu, S.-C., et al., Development of loop-mediated isothermal amplification (LAMP) assays for the rapid detection of allergic peanut in processed food. *Food chemistry*, 2018. 257: p. 67-74.

22. Hahn, J., et al., Development of a portable lab-on-a-valve device for making primary diagnoses based on gold-nanoparticle aggregation induced by a switchable linker. *RSC Advances*, 2020. 10(52): p. 31243-31250.

23. Hahn, J., et al., A Switchable Linker-Based Immunoassay for Ultrasensitive Visible Detection of Salmonella in Tomatoes. *Journal of food science*, 2017. 82(10): p. 2321-2328.

24. You, Y., et al., Bifunctional linker-based immunosensing for rapid and visible detection of bacteria in real matrices. *Biosensors and Bioelectronics*, 2018. 100: p. 389-395.

25. Lim, S., et al., Enhancing nanoparticle-based visible detection by controlling the extent of aggregation. *Scientific reports*, 2012. 2(1): p. 1-6.

26. Holzhauser, T., et al., Are current analytical methods suitable to verify VITAL® 2.0/3.0 Allergen Reference doses for EU Allergens in Foods? *Food and Chemical Toxicology*, 2020: p. 111709.

27. Bastús, N.G., J. Comenge, and V. Puntes, Kinetically controlled seeded growth

synthesis of citrate-stabilized gold nanoparticles of up to 200 nm: size focusing versus Ostwald ripening. *Langmuir*, 2011. 27(17): p. 11098-11105.

28. Walczyk, N.E., et al., Peanut protein extraction conditions strongly influence yield of allergens Ara h 1 and 2 and sensitivity of immunoassays. *Food chemistry*, 2017. 221: p. 335-344.

29. Chivers, C.E., et al., A streptavidin variant with slower biotin dissociation and increased mechanostability. *Nature methods*, 2010. 7(5): p. 391.

30. Huang, Y., M.C. Bell, and I.I. Suni, Impedance biosensor for peanut protein Ara h 1. *Analytical chemistry*, 2008. 80(23): p. 9157-9161.

31. Remington, B.C., et al., Updated population minimal eliciting dose distributions for use in risk assessment of 14 priority food allergens. *Food and Chemical Toxicology*, 2020. 139: p. 111259.

32. Sendroiu, I.E., S.F. Mertens, and D.J. Schiffrin, Plasmon interactions between gold nanoparticles in aqueous solution with controlled spatial separation. *Physical Chemistry Chemical Physics*, 2006. 8(12): p. 1430-1436.

33. Huang, C.-C., et al., Aptamer-modified gold nanoparticles for colorimetric determination of platelet-derived growth factors and their receptors. *Analytical chemistry*, 2005. 77(17): p. 5735-5741.

34. Pavlov, V., et al., Aptamer-functionalized Au nanoparticles for the amplified optical detection of thrombin. *Journal of the American Chemical Society*, 2004. 126(38): p. 11768-11769.

35. Blanco, P.M., et al., Brownian dynamics computational model of protein diffusion in crowded media with dextran macromolecules as obstacles. *Entropy*, 2017. 19(3): p. 105.

36. Mir, M.U.H., et al., Molecular interaction of cationic gemini surfactant with bovine

serum albumin: A spectroscopic and molecular docking study. *Process Biochemistry*, 2014. 49(4): p. 623-630.

37. Costa, J., et al., Are physicochemical properties shaping the allergenic potency of plant allergens? *Clinical Reviews in Allergy & Immunology*, 2020: p. 1-27.

38. Keum, E.-H., S.-I. Lee, and S.-S. Oh, Effect of enzymatic hydrolysis of 7S globulin, a soybean protein, on its allergenicity and identification of its allergenic hydrolyzed fragments using SDS-PAGE. *Food Science and Biotechnology*, 2006. 15(1): p. 128-132.

39. Boualeg, I. and A. Boutebba, Purification of water soluble proteins (2S albumins) extracted from peanut defatted flour and isolation of their isoforms by gel filtration and anion exchange chromatography. *Scientific Study & Research. Chemistry & Chemical Engineering, Biotechnology, Food Industry*, 2017. 18(2): p. 135.

40. Liu, C., et al., Optimization of extraction and isolation for 11S and 7S globulins of soybean seed storage protein. *Food Chemistry*, 2007. 102(4): p. 1310-1316.

Chapter III. Development of novel aptamer-based switchable linker and complementary DNA modified gold nanoparticle

III-1. Introduction

The development of a colorimetric detection method using gold nanoparticles plays an important role in food fields [1-4]. Because it has the advantage of being able to easily determine the detection signal, colorimetric detection methods have been developed for various targets such as harmful microorganisms, allergens, toxic substances, heavy metals, pesticides, antibiotics, and adulterated foods [5-13]. Among these detection methods, the method using a switchable linker (SL, i.e. bifunctional linker) has another advantage. Like other gold nanoparticle colorimetric detection methods, the detection method using SL has the advantage of being able to rapidly and sensitively detect. And it also exhibits the detecting result without any other analytical instruments. In addition, when SL is used, it induces larger-scale aggregation than other detection methods, not only changes in color by aggregation, but also forms huge clusters to cause precipitation. The precipitation of these particles is easier to identify than the color change. Therefore, it has the advantage of giving a more reliable and strong visual signal than other colorimetric detection methods. Moreover, one linker generally can induce bridging between two gold nanoparticles, whereas SL is designed to form aggregates at the same time with a large amount of gold nanoparticles, so it reacts more sensitively to the change of the linker by the target. Improved overall sensitivity. Based on this theoretical background, so far, it has been shown that sensitive detection is possible for various detection targets such as microorganisms, allergens, and PSA [14-19].

In the previous studies, SL was designed based on antibodies. An antibody based SL is composed of antibodies with many biotins labeled on the surface. The antibody can selectively recognize the target and biotins on antibody can bind streptavidin on the surface of

the gold nanoparticles. When this biotinylated antibody reacts with gold nanoparticles which is decorated with many streptavidins at a specific ratio, it forms huge clusters and causes precipitation. However, when the biotinylated antibody recognizes the target, the steric hindrance prevents the binding between biotin and streptavidin, which causes the loss of the ability to form clusters of gold nanoparticles, so this is called a switchable linker. The colorimetric detection method using this antibody-based SL shows high sensitivity and selectivity because of an antibody, and a fast aggregation rate resulting from the affinity of biotin and streptavidin. However, there are disadvantages as well. First, it is easy to mass-produce one antibody targeting one target, but it is relatively difficult to produce a variety of antibodies targeting various targets in a small amount. Second, to maintain the three-dimensional structure of antibody, refrigeration or freezing storage is essential. Finally, since the process of functionalizing with biotin is difficult and the yield is low, there is a cost burden issue. Therefore, in order to compensate for the shortcomings of such antibody-based SL, it is necessary to design a new type of SL and to develop a detection method using it.

An aptamer, DNA sequence that selectively recognizes a target material, has been highlighted as a substance that can replace an antibody [6, 20-23]. Because aptamer is DNA sequence, they are very stable than antibodies and It can be produced quickly and easily using enzymes. In addition, it is suitable for development of novel detection method because it can be produced by utilizing DNA sequences that have already been studied for specific binding capacity. In this study, a new form of SL and gold nanoparticle was designed. And a novel detection method was proposed utilizing these SL and gold nanoparticle.

III-2. Materials and Methods

III-2.1 Materials

LUDOX AS-30 silica (ammonium salt, 30 wt% in water), acetic acid, glutathione, tetrachloroauric(III) acid trihydrate, chloroauric acid, 6-Mercapto-1-hexanol, gliadin from wheat and thiolated polyethylene glycol (PEG-SH) were purchased from Sigma Aldrich (St. Louis, MO, USA). Ethyl alcohol was purchased Duksan pure Chemical (Seoul, Korea). Glutaraldehyde and 3-aminopropyltriethoxysilane(APTES) and ethanolamine were purchased from TCI (Tokyo, Japan). Gliadin aptamer (5′-(NH_2)-$(CH_2)_6$-TTT TTC TAC ACA TGT CTG AAT GCC-3′) and its part complementary DNA strand (5′-HS-$(CH_2)_6$-TTT TTG GCA TTC AGA CAT GTG TAG-3′.) reported by Svigelj et al. [24] were synthesized by bioneer Coperation (Daejeon, Korea).

III-2.2Instrumentation

Absorbance measurements were performed on a UV-1700 spectrophotometer (Shimadzu, Kyoto, Japan). The pH values of all buffer solutions were determined using the Professional Meter PP-15 (Satorious, Göttingen, Germany). Particle sizes and distributions were determined by dynamic light scattering (DLS) with a Zetasizer Nano-ZS 90 (Malvern, Worcestershire, UK).

III-2.3 Preparation of gold nanoparticle (AuNP)

Gold nanoparticles (AuNP), 13 nm in diameter, were synthesised according to the

method established by Turkevich et al. [25]. Briefly, the AuNPs were synthesized by adding 5 mL of thrisodium citrate solution (38.8 mM) rapidly to a boiling solution of $HAuCl_4$ (1.0 mM, 50 mL) and stirred for 30 min to form a wine-red solution. Resulting solution was cooled to room temperature while being stirred continuously. Ultimately, AuNP 13 nm in diameter were obtained and stored at 4 °C until further use. All glassware used in the experiment was thoroughly washed with freshly prepared aqua regia (HNO_3/HCl = 1:3) prior to use. The particle sizes of the AuNP were determined using an ultraviolet/visible (UV/Vis) spectrophotometer and DLS.

III-2.4 Preparation of aptamer and complementary DNA (cDNA) modified gold nanoparticles

To prepare DNA−AuNP conjugates with the pH-Assisted method, first, various quantity of thiolated DNA stock solution (100 μM in 10 mM Tris-HCl buffer, pH 8.0 with 0.1 mM EDTA) was treated with TCEP (100x) for 1 hr tor cleave the disulfide bond. The resulting solution was added into synthesized AuNP solution (DNA:AuNP ratio = 0:1 – 150:1), and then mixture was heated to 60°C in water bath. Second, pH 3 sodium citrate buffer (100 mM) was introduced to the AuNPs solution with a final concentration of 10 mM. After a 5 min incubation at 60°C temperature, the pH of the AuNP solution was adjusted back to neutral by adding 600 mM HEPES buffer to a final HEPES concentration of 30 mM (pH 7.4). The sample was cooled to room temperature for another 15 min. Finally, the thiol-DNA−AuNPs conjugate was centrifuged at 16,000xg for 30 min, and the supernatant was removed. Finally, the precipitate was washed with 5 mM HEPES to remove free DNA. This centrifugation and washing procedure was repeated 3 times to ensure complete removal of free thiol-DNA, and the

conjugate was kept in 5 mM HEPES buffer for further use.

III-2.5 Removal of Nonspecific DNA Adsorption on surface of AuNP

Thiolated PEG (PEG-SH), 6-Mercapto-1-hexanol (MCH) and glutathione (GSH) were used to displace the nonspecific adsorption of thiolated DNAs on AuNP surfaces, so as to improve the hybridization capacity of the adsorbed DNA strands with their complementary strands. The synthesized SH-DNA modified AuNP nanoconjugates were exposed to MCH in water at a final concentration of 10 μM, with a reaction time of 1 min. Reactions were halted by washing with 2× volume of ethyl acetate, which extracts excess MCH out of the aqueous solution. Then, the conjugates were centrifuged at 14 000 rpm at room temperature for 10 min. The precipitates were resuspended in 50 mM Tris-HCl buffer (pH) with 300 mM NaCl for further use. The MCH extraction using ethyl acetate is improtant since it allows control of reaction time, which is essential for avoiding complete displacement of the oligo and ligand [26]. Glutathione and PEG-SH solution (100 mM) were respectively introduced to the DNA-AuNP conjugate solution with final concentration of 10 mM and incubated for 10 min. Reaction was halted by centrifugation at 16,000xg for 30 min at room temperature. The precipitates were resuspended in 50 mM Tris-HCl buffer (pH 7.4). This centrifugation and washing procedure was repeated 3 times to ensure complete removal of free glutathione, and the conjugate was kept in 50 mM Tris-HCl buffer (pH) with 300 mM NaCl for further use.

III-2.6 Synthesis of nanoparticles functionalized with amino groups

The method of Gerrans and coworkers was adopted for amino group modifications on Silica nanoparticle [27]. LUDOX AS-30 silica nanoparticles (SNP), 20 mL was added to a

solution contacting ethanol (100 mL), water (60 mL) and acetic acid (60 mL). To this solution was added APTES (1.2 mL, 5.2 mmol) followed by stirring at 80°C under N_2 for 48 h. Then, the functionalized silica nanoparticles were isolated by centrifugation (relative centrifugal force, 29,720, 2 h), and the supernatant was decanted, the resulting solid washed with ethanol, and centrifuged again for 2 h. This cycle was repeated thrice more after which the white solids were vacuum dried at 70°C overnight. Finally, the dried SNP-APTES was resuspended in HEPES buffer (20 mM, pH 7.4) for further use.

III-2.7 Removal of Nonspecific DNA Adsorption on surface of SNP

Ethanolamine and glutathione were used to displace the nonspecific adsorption of thiolated DNAs on AuNP surfaces, so as to improve the hybridization capacity of the adsorbed DNA strands with their complementary strands. Ethanolamine and glutathione solution (100 mM) were respectively introduced to the DNA-SNP conjugate solution with final concentration of 10 mM and incubated for 10 min. Reaction was halted by centrifugation at 16,000xg for 30 min at room temperature. The precipitates were resuspended in 50 mM Tris-HCl buffer (pH 7.4). This centrifugation and washing procedure was repeated 3 times to ensure complete removal of free glutathione, and the conjugate was kept in 50 mM Tris-HCl buffer (pH) with 300 mM NaCl for further use.

III-3. Results and Discussion

III-3-1. Hypothesised structure of aptamer modified switchable linker and complementary nanoparticle

As shown in Figure III-1, SL was designed in the form of functionalizing a number of aptamer that can selectively recognize targets into nanoparticles. The SL must first fulfill two functions, first it needs the ability to form aggregate a large number of gold nanoparticles, and second it loses the ability to aggregate gold nanoparticles by recognizing the target, ie, Switch-off must be possible. In the case of antibody-based SL, the ability to aggregate gold nanoparticles was imparted by labeling a large number of biotins into the antibody so that it could specifically bind to streptavidin coated on the surface of the gold nanoparticles. Then, a switch-off method was used for the steric hindrance caused by the antibody recognizing the target, which inhibits the binding between streptavidin and biotin.

Unlike antibody based SL, which has separate parts that induce aggregation between gold nanoparticles and parts that recognizes targets, in aptamer based SL, aptamer have both function that binds between gold nanoparticles and recognizes targets. The aptamer which is functionalized on the surface of silica nanoparticles, forms a double helix with the complementary DNA aptamer on the surface of gold nanoparticles. Since a large number of aptamers are functionalized on the surface of the silica nanoparticles, the plurality of gold nanoparticles is simultaneously bonded to form aggregates. And, when the aptamer recognizes the target, it prevents the formation of a double helix structure between aptamer and complementary DNA, and the function as a linker is switched-off. Compared to antibody-based SL, which is difficult to regulate the number of functional groups that induce particle

aggregation or recognize the target, aptamer based SL could easily adjust the number of aptamer, it has the advantage of being easy to study the effect of the number and density of functional group on the detection system.

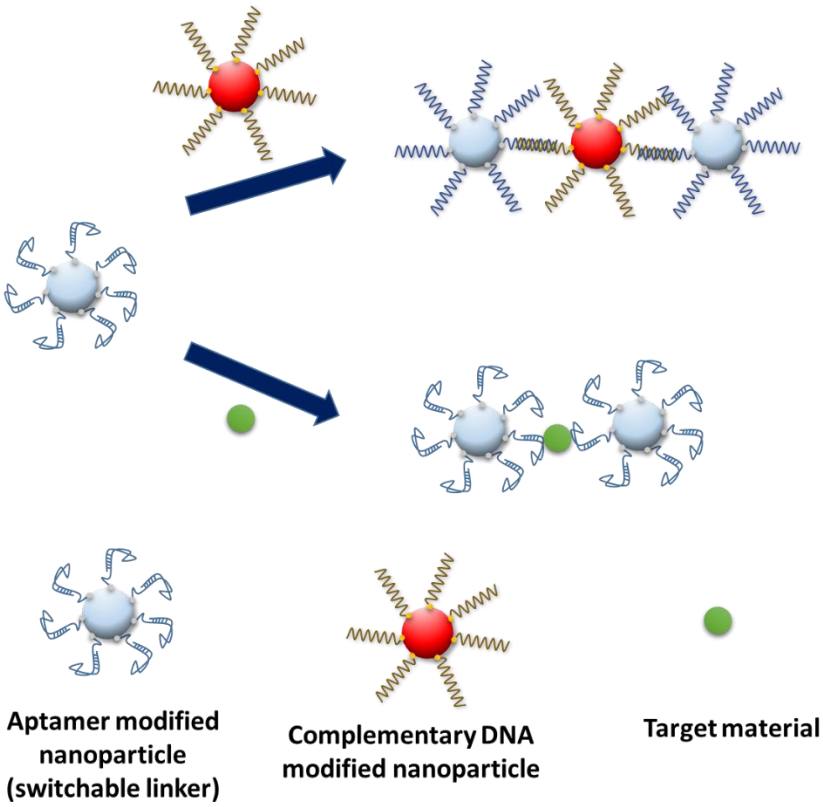

Figure III -1. Schematic diagram of the crosslinking reaction of the aptamer modified nanoparticles as SL with the complementary DNA modified nanoparticles or target materials.

III-3-2. DNA modification on the surface of AuNP

To modify the DNA on the AuNP surface, the salt aging method and the low-pH method were compared. It is widely known that gold reacts selectively with sulfur. Therefore, it is possible to selectively mold on the surface of gold nanoparticles by using a DNA sequence consisting of a thiol group at the end. However, only mixing gold nanoparticles with a thiol-terminal DNA sequence results in poor molding efficiency. At this time, various methods such as a method of gradually increasing the salt concentration, a method of lowering the pH, and a method of heating to a high temperature have been studied as a method of accelerating the bonding of sulfur on the surface of the gold nanoparticles. First, the method that has been used a lot traditionally is the salt aging method. When the salt concentration of the gold nanoparticle-DNA mixture is increased, the bonding of the gold nanoparticle surface and the sulfur is accelerated. However, if the salt concentration is rapidly raised, the surface of the gold nanoparticles becomes insane and irreversible aggregation by the salt is induced before it is stabilized with DNA, so the surface modification of the DNA is gradually increased by gradually adding a high concentration salt solution over time. Although this method has been studied the most, it has a disadvantage that it takes a lot of time compared to other methods. In order to compensate for the shortcomings of salt aging, a method of adding polymer PEG to a mixture has been recently announced as a method of maintaining dispersion stability of gold nanoparticles while accelerating the surface modification of DNA in the presence of a high concentration of salt [28]. The pH method is a relatively recently developed method in which a citrate buffer of pH 3.0 is added to the mixture of gold nanoparticles and DNA to lower the pH and neutralize with HEPES buffer after 5 minutes to terminate the reaction [29]. In this method, the reaction can be terminated in just 5 minutes, while the salt aging method proceeds

over several hours. In order to check whether there is a difference between the produced particles, the surface of the gold nanoparticles was modified using the salt aging method and the pH method, respectively. All of the produced particles showed a peak at 522.5 nm. This means that both nanoparticles have modified with the similar number of DNA. And, when the gold nanoparticles were resuspended in reaction buffer (pH 7.4 of 50 mM Tric-HCl buffer with 300 mM NaCl) after repeated centrifugation three times, both particles showed equally high stability. However, in the case of salt aging, the viscosity of the solution was relatively high due to the PEG added to the solution. As a result, during repeated centrifugation and removal of the supernatant, the salt aging method lost a relatively greater amount of gold nanoparticles than the pH method. It results in a lower yield of particles. Finally, there was no difference in the particles produced in both methods, and the pH method was simpler and showed a high particle yield, so this was adopted and used for the surface modification of gold nanoparticles later.

III-3-3. Reducing nonspecific DNA adsorption on surface of AuNP

When the DNA on the surface of the gold nanoparticles is modified, unwanted non-specific adsorption occurs. This is not as strong as the gold-sulfur bond because the nitrogen possessed by DNA has a positive charge, but it is possible to cover the surface of the gold nanoparticles, which is a factor that inhibits the reaction with the complementary DNA or the target to be recognized [29]. The simplest way to prevent such non-specific adsorption is to react a large number of DNA with gold nanoparticles so that a specific reaction occurs sufficiently. However, when an excessive amount of DNA is reacted to the gold nanoparticles, the DNA density on the surface of the particles becomes excessively high, indicating steric

hindrance, which degrades the efficiency of reaction with the complementary sequence [29]. Therefore, in order to remove non-specific adsorption on the surface of gold nanoparticles and maintain an appropriate level of DNA density, a method of modifying the surface of gold nanoparticles that did not react with a thiol group with a material having a higher affinity for gold than the DNA sequence is used. Commonly used materials include MCH, PEG formed with a thiol group at the end, and glutathione, a short peptide including cysteine.

The above-mentioned MCH, thiolated PEG-5000-SH and glutathione were reacted to gold nanoparticles modified with the various number of aptamer or cDNA, and the stability. First, in the case of the MCH-treated particles, the gold nanoparticles:DNA ratio of 40:1 or higher was required to secure stability in the 300 mM NaCl solution (figure III-2A). This was different from the stable gold nanoparticles treated with a relatively low particle:DNA ratio of 25:1 in the case of GSH (figure III-2B). When the zeta potetial of the two particles was measured, the GSH-treated gold nanoparticles showed -20.8 mV, while the MCH-treated gold nanoparticles showed a much smaller zeta potential as -10.2 mV (Table. III-1.). When AuNP is treated with MCH consisting of 6 carbons, except for thiol, the hydrophobicity is relatively strong, and the particle chage appears to be relatively low. In the case of PEG-SH, the particle was shown lowest zeta potential (-5.0 mV), but it also had higher stability than MCH treated particle because of their steric hindrance. On the other hand, this seems to be because PEG of sufficient length imparts particle stability through steric hindarance of PEG itself irrespective of the charge of DNA (Figure III-3).

Gold nanoparticles molded with aptamer and cDNA were treated with MCH, GSH, and PEG-SH to react the particles at different ratios and compared their ability to form aggregates. When the gold nanoparticles molded with MCH and GSH reacted 1:1 with the

complementary particles, it was confirmed that the fastest aggregates were formed and precipitated (figure III-3). However, the reaction between the particles treated with MCH took place faster than the reaction between the particles treated with GSH, and aggregation was observed even in a reaction ratio other than 1:1. Since the gold nanoparticles treated with MCH have poor stability, it appears to be a result of nonspecific aggregation. For the same reason, the loss of particles over time was also the greatest in the particles treated with MCH. On the other hand, in the case of gold nanoparticles treated with PEG-SH, it was confirmed that precipitation did not occur in all areas regardless of the ratio between the reacted gold nanoparticles. This seems to be because steric hindrance caused by PEG, which is relatively longer than the previous MCH and GSH, also interferes with the formation of hepatic duplex of DNA on the surface of gold nanoparticles.

As a result, the particles treated with MCH have poor stability of the particles, and in the case of PEG, the stability of the particles is good, but the aggregation reaction itself is inhibited. I did. Therefore, GSH-treated particles were selected and used in subsequent experiments.

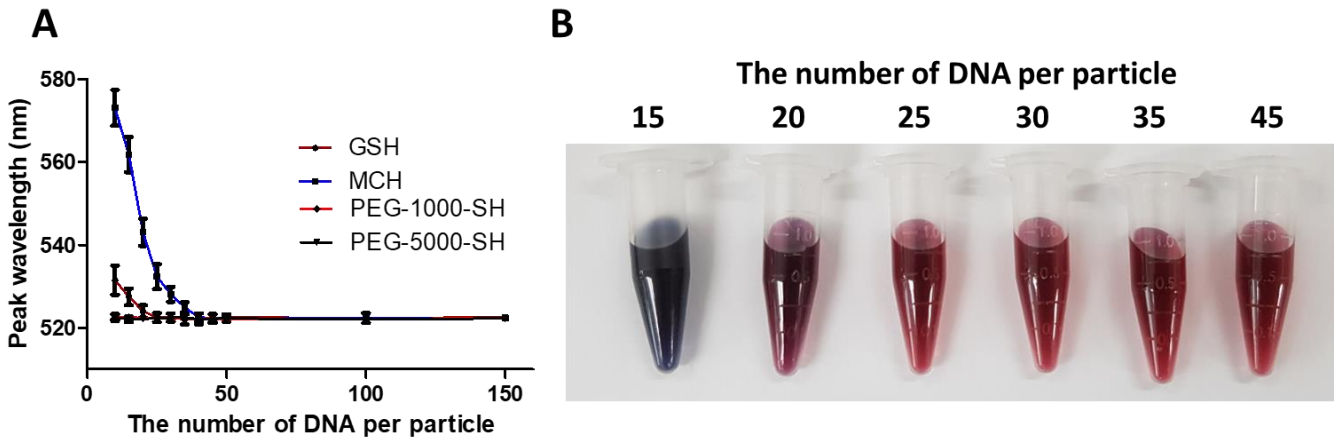

Figure. III-2. Colloidal stability of the AuNP by the different surface concentrations of DNA. (A) The peak wavelength results of AuNP surface-modified with the different non-specific adsorption prevention materials: GSH, MCH, PEG-1000-SH and PEG-5000-SH; (B) The appearance of GSH-backfilling-AuNP depending on the number of the DNA.

Table. III-1. Zeta potential and particle loss of the AuNP surface-modified with the different non-specific adsorption prevention materials: GSH, MCH, and PEG-5000-SH

Non-specific adsorption prevention material	Zeta potential (mV)	Particle loss for 28 days (%)
6-mercpato-1-hexanol	-10.2 ± 0.8	5 ± 2
Glutathione	-20.8 ± 2.1	40 ± 6
Thiolated polyethyleneglycol (M.W 5000)	-5.0 ± 0.3	25 ± 4

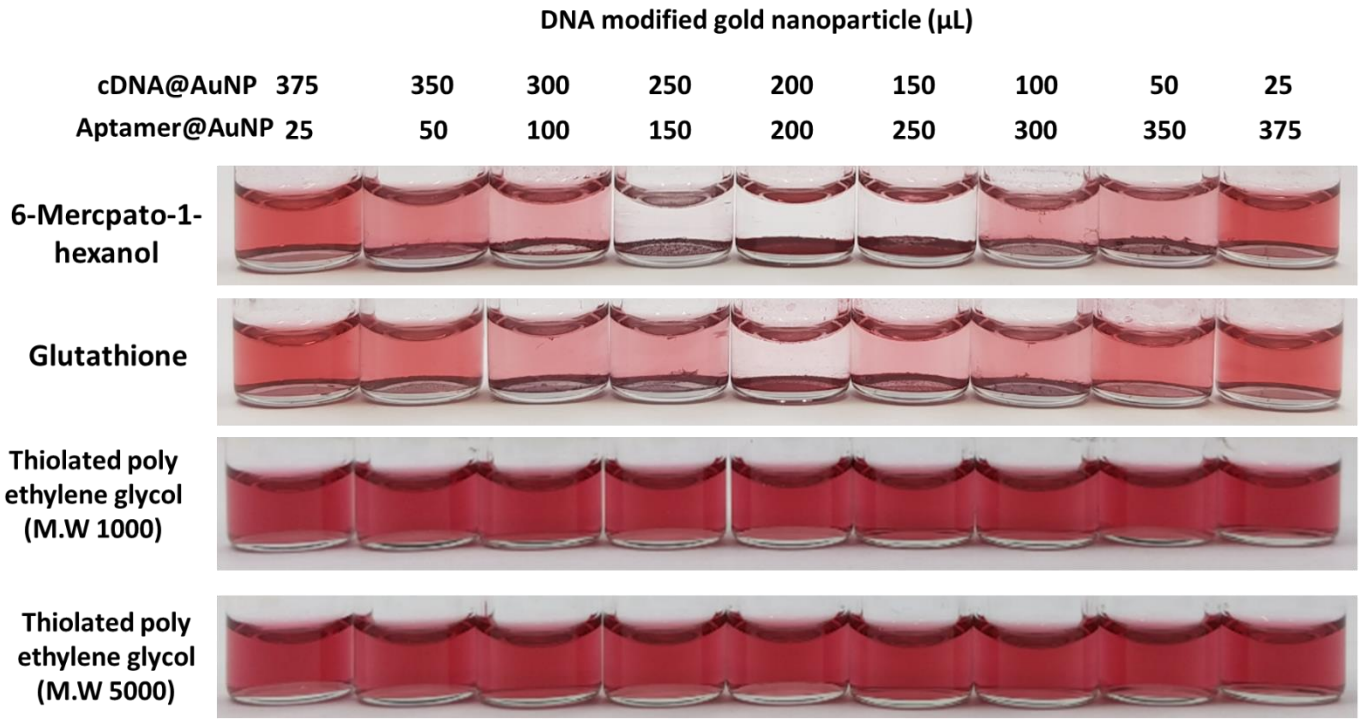

Figure. III-3. The visible signal result by aggregation and/or precipitation of the AuNP modified with the different non-specific adsorption prevention materials: GSH, MCH, PEG-1000-SH and PEG-5000-SH.

III-3-4. Selection of core nanoparticle material for switchable linker development

The SL linker-based colorimetric detection method consists of a series of linkers of different concentrations and gold nanoparticles of a specific concentration molded to form aggregates by reacting with the linkers, respectively. Gold nanoparticles and linkers form the largest aggregates at a specific ratio, and the ratio of linkers that recognize targets changes, but when reacting with a series of linkers of different concentrations, the change in the ratio is the linker concentration where precipitation occurs most easily. Appears as a change of. In other words, in order to confirm that the aggregate is well formed and precipitated, the linker itself should not show color in the solution. If the linker remaining without reacting with the gold nanoparticles shows a color in the solution, it is difficult to distinguish whether this color is the color that appears due to the remaining gold nanoparticles or the linker remains, which makes it easy to visually determine the presence of the target. It is not suitable for developing a colorimetric detection method. Therefore, unlike gold nanoparticles, a probe that has the purpose of indicating color, SL does not absorb visible light, so it is better not to confuse the system.

Like gold nanoparticles, methods of manufacturing metal nanoparticles using silver, platinum, or various alloys have been studied and

used. These metal nanoparticles have a diameter of about 10 to 100 nm like gold nanoparticles, so it is possible to make them into a small size with good dispersibility. However, although different from gold nanoparticles, they each exhibit specific colors by absorbing light in the visible range of different wavelengths. On the other hand, in the case of silica nanoparticles, the manufacturing method and surface molding method have been studied a lot, so it is easy to make nanoparticles having a diameter of several tens of nanometers like metal nanoparticles. Also, unlike metals, nano-sized particles do not absorb visible light, so they are suitable for use as a core of SL. In addition, it is an advantage that metal nanoparticles do not have the fact that there is no worry about toxicity, so that it is widely used in food manufacturing processes such as enzyme fixing. For this reason, silica nanoparticles were selected as the core of SL.

III-3-5. DNA modification on the surface of SNP

In the case of silica nanoparticles, the stober method is most commonly known as a synthesis method. In the case of the stober method using acetic acid, water, and alcohol, it is possible to control the size of nanoparticles by changing the type of alcohol used during synthesis. In general,

in order to produce SNPs of 100 nm or less, methyl alcohol must be used, but there is a disadvantage that purification is difficult and there is a risk due to residual methyl alcohol [30]. For this reason, silica nanoparticles with a diameter of 12 nm whose surface is stabilized with ammonium ion were purchased and used in the experiment. In the case of the purchased SNP, since the diameter is 12 nm and the surface is composed of hydroxyl groups, it is necessary to substitute a functional group suitable for surface modification [27]. APTES is a material in which one functional group of TEOS, a basic material for synthesizing silica nanoparticles, is substituted from a hydroxyl group to an amine group, and is used to replace the surface of silica nanoparticles with an amine group. Unlike the hydroxyl group, the amine group has a positive charge, so whether or not it has been substituted can be confirmed by the zeta potential. The zeta potential of silica nanoparticles before surface substitution with APTES was -11.2 mV. On the other hand, it was confirmed that the zeta potential of the silica nanoparticles after substitution was changed to +30 mV. Then, the amine groups on the surface of the particles were activated by a bifunctional agent, glutaraldehyde. Unlike when substituted with an amine group, SNPs with glutaraldehyde surface-substituted lost high electrostatic repulsion and formed gels to precipitate. However, when the amine labeled aptamer was reacted with the

glutaraldehyde of this particle, it was confirmed that DNA with a long length gave steric hindrance to the silica nanoparticles and dispersed again (Figure III-4B). Finally, blocking agents were additionally reacted to block the functional groups of glutaraldehyde remaining on the surface without binding to the aptamer. If the functional group of glutaraldehyde remains on the surface of the particle, there is a possibility that it may bind to a polypeptide or protein in food that has an amine group or a thiol group. In addition, as with the phenomenon of gold nanoparticles, the DNA sequence of the aptamer causes non-specific adsorption to the particle surface by electrostatic attraction with glutaraldehyde, which can lead to a decrease in the stability of the particles and the ability to form aggregates. Therefore, glutaraldehyde on the surface of silica nanoparticles need to be properly blocked. In order to remove residues on the surface of the silica nanoparticles and prevent non-specific binding, GSH and ethanolamine were introduced as blocking agents, and the stability and reactivity of each particle were examined. In the case of ethanolamine, when used as a blocking agent, it exhibited high hydrophobic properties, leading to nonspecific aggregation between particles. As can be seen from the figure 4, the silica nanoparticles blocked with ethanolamine showed that most of the particles formed large aggregates. On the other hand, the silica nanoparticles blocked with GSH showed a low zeta potential of -20 mV, like

the gold nanoparticles, and it was confirmed that the particles exhibited good dispersibility in DLS analysis (Figur. III-4C).

III-3-6. Determination of the aggregate-forming ability of the bifunctional linker

To confirm the ability of aptamer based bifunctional linkers to induce aggregation, aptamer functionalized silica nanoparticles (Apt@SNP) and complementary DNA functionalized gold nanoparticles (cDNA@AuNP) was reacted with various concentrations. First, in each vial, it was mixed 200 ul of Apt@SNP at various concentrations ranging from 0.01 to 1.0 mg/mL and 200 ul of 16.2 nM (Abs. 4.0 at 522 nm) cDNA@AuNP. The mixture was shaken by a vortaxer at room temperature. Then, the formation of the precipitation region was observed at 5 minute intervals. As a result, as shown in Figure III-5, the precipitation was completed in just 15 minutes and the transparent area was observed, which was clearly visible. This indicates that the DNAs functionalizing of the gold nanoparticles and the silica nanoparticles generate complementary bonds with each other. And as confirmed earlier, cDNA@AuNP and Apt@SNP are stably dispersed when they are not mixed with each other. Taken together, it was confirmed that a linker capable of

selectively binding to gold nanoparticles and successfully forming gold nanoparticle aggregates.

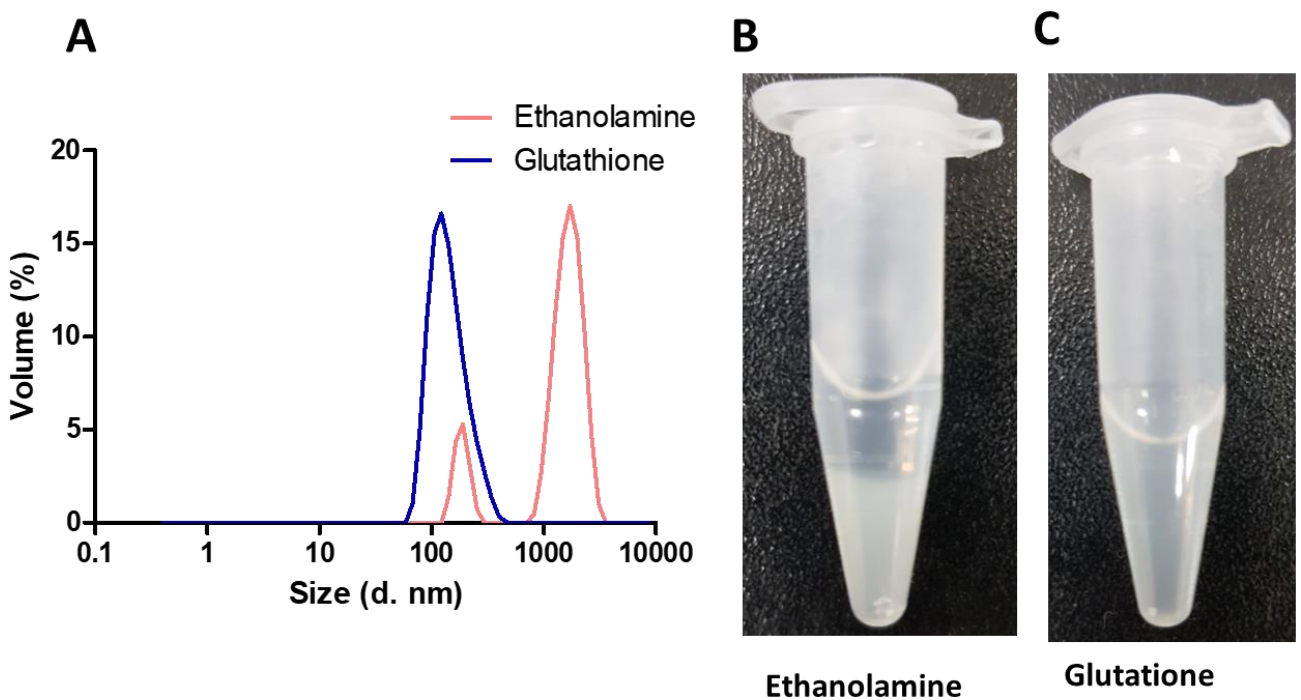

Figure III-4. The dispersion stability of the SNP. (A) Volume-size distribution of the surface-modified SNP; Appearance of the SNP modified by (B) ethanolamine and (C) GSH as a backfilling material.

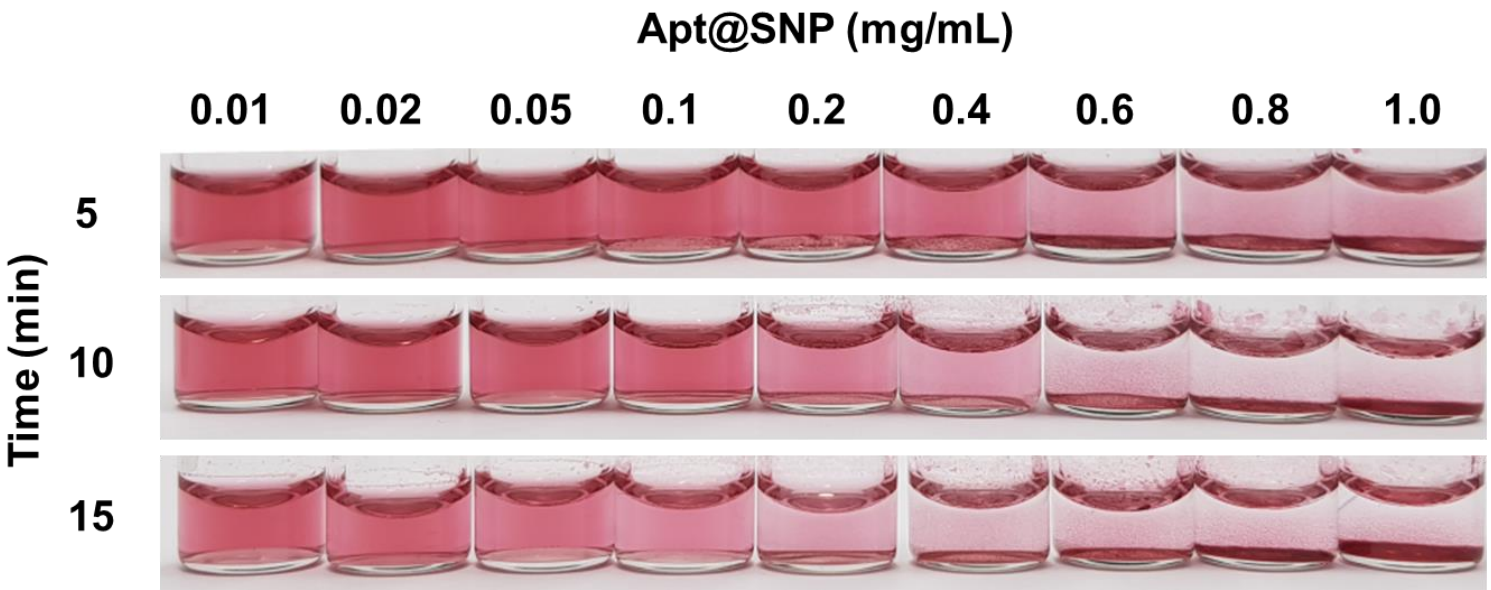

Figure III-5. Color of the AuNPs with different amounts of Apt@SNP (0.01 to 1.0 mg/mL) as function of time.

III-4. Conclusions

In previous studies, antibody-based SL has been effectively used to develop detection methods for various targets such as microorganisms, allergens, and cancer biomarkers. However, there are difficulties in developing a detection method with antibody-based SL, such as the price of the antibody or difficulty in manufacturing and storage, so it was necessary to develop a new type of switchable linker. In this study, a new SL using aptamer, a fragment of DNA that is capable of recognizing a specific substance was devised. And functionalizing method for gold nanoparticle with complementary DNA and aggregation system utilizing SL were devised as well. In addition, in order to optimize SL and gold nanoparticles, a method of decorating DNA on each surface and blocking with appropriate material were screened. As a result, in the case of gold nanoparticles, it was most appropriate to modify DNA having thiol groups on the particle surface by the pH method and to block non-specific adsorption with GSH. And in the case of SL, silica nanoparticles were selected as core nanoparticles and APTES was used to aminate its surface. Glutaraldehyde was used as a bifunctional agent to effectively bind the aminated aptamer to the surface of silica nanoparticles. Finally, like gold nanoparticles, dispersion stability was enhanced by using GSH. The developed SL and gold nanoparticles maintained good dispersibility, respectively. And when they reacted with each other, they showed forming huge aggregates and precipitating, similar to the previous SL and gold nanoparticles. Through the development of this new type of SL, it is expected to be possible to develop a colorimetric detection method that easily and quickly detects various harmful microorganisms and substances in food.

III-5. References

1. Chen, H., K. Zhou, and G. Zhao, Gold nanoparticles: From synthesis, properties to their potential application as colorimetric sensors in food safety screening. *Trends in Food Science & Technology*, 2018. 78: p. 83-94.
2. Jazayeri, M.H., et al., Colorimetric detection based on gold nano particles (GNPs): An easy, fast, inexpensive, low-cost and short time method in detection of analytes (protein, DNA, and ion). *Sensing and bio-sensing research*, 2018. 20: p. 1-8.
3. Liu, G., et al., Application of gold-nanoparticle colorimetric sensing to rapid food safety screening. *Sensors*, 2018. 18(12): p. 4166.
4. Pissuwan, D., et al., Single and multiple detections of foodborne pathogens by gold nanoparticle assays. *Wiley Interdisciplinary Reviews: Nanomedicine and Nanobiotechnology*, 2020. 12(1): p. e1584.
5. Schofield, C.L., R.A. Field, and D.A. Russell, Glyconanoparticles for the colorimetric detection of cholera toxin. *Analytical chemistry*, 2007. 79(4): p. 1356-1361.
6. Xue, X., F. Wang, and X. Liu, One-step, room temperature, colorimetric detection of mercury (Hg2+) using DNA/nanoparticle conjugates. *Journal of the American Chemical Society*, 2008. 130(11): p. 3244-3245.
7. Bala, R., et al., Ultrasensitive aptamer biosensor for malathion detection based on cationic polymer and gold nanoparticles. *Biosensors and Bioelectronics*, 2016. 85: p. 445-449.
8. Kumar, N., et al., Colorimetric determination of melamine in milk using unmodified silver nanoparticles. *Spectrochimica Acta Part A: Molecular and Biomolecular Spectroscopy*, 2016. 156: p. 89-97.

9. Zhang, Y., et al., Colorimetric detection based on localised surface plasmon resonance of gold nanoparticles: merits, inherent shortcomings and future prospects. *Talanta*, 2016. 152: p. 410-422.

10. Fang, C., et al., Gold nanoparticle-based optical sensors for selected anionic contaminants. *TrAC Trends in Analytical Chemistry*, 2017. 86: p. 143-154.

11. Liu, G., et al., Determination of triazole pesticides in aqueous solution based on magnetic graphene oxide functionalized MOF-199 as solid phase extraction sorbents. *Microporous and Mesoporous Materials*, 2018. 270: p. 258-264.

12. Malachová, A., et al., Advanced LC–MS-based methods to study the co-occurrence and metabolization of multiple mycotoxins in cereals and cereal-based food. *Analytical and bioanalytical chemistry*, 2018. 410(3): p. 801-825.

13. Li, J., et al., An electrochemiluminescence aptasensor based on Ru (bpy) 3 2+ encapsulated titanium-MIL-125 metal-organic framework for bisphenol A assay. *Microchimica Acta*, 2020. 187(4): p. 1-8.

14. Hahn, J., et al., Development of a portable lab-on-a-valve device for making primary diagnoses based on gold-nanoparticle aggregation induced by a switchable linker. *RSC Advances*, 2020. 10(52): p. 31243-31250.

15. Hahn, J., et al., Colorimetric switchable linker-based bioassay for ultrasensitive detection of prostate-specific antigen as a cancer biomarker. *Analyst*, 2019. 144(14): p. 4439-4446.

16. Hahn, J., et al., A Switchable Linker-Based Immunoassay for Ultrasensitive Visible Detection of Salmonella in Tomatoes. *Journal of food science*, 2017. 82(10): p. 2321-2328.

17. Kim, E., et al., Visible on-site detection of Ara h 1 by the switchable-linker-mediated

precipitation of gold nanoparticles. *Food Chemistry*, 2021. 352: p. 129354.

18. Lim, S., et al., Enhancing nanoparticle-based visible detection by controlling the extent of aggregation. *Scientific reports*, 2012. 2(1): p. 1-6.
19. You, Y., et al., Bifunctional linker-based immunosensing for rapid and visible detection of bacteria in real matrices. *Biosensors and Bioelectronics*, 2018. 100: p. 389-395.
20. Perlman, J., Rapid Colorimetric Determination of Lead in Maple Syrup. *Industrial & Engineering Chemistry Analytical Edition*, 1938. 10(3): p. 134-135.
21. Moine, H., et al., The RNA binding site of S8 ribosomal protein of Escherichia coli: Selex and hydroxyl radical probing studies. *RNA*, 1997. 3(3): p. 255-268.
22. Bai, W., et al., Gold nanoparticle–based colorimetric aptasensor for rapid detection of six organophosphorous pesticides. *Environmental toxicology and chemistry*, 2015. 34(10): p. 2244-2249.
23. Chu, W., et al., A biomimetic sensor for the detection of lead in water. *Biosensors and Bioelectronics*, 2015. 67: p. 621-624.
24. Svigelj, R., et al., Truncated aptamers as selective receptors in a gluten sensor supporting direct measurement in a deep eutectic solvent. *Biosensors and Bioelectronics*, 2020. 165: p. 112339.
25. Frens, G., Controlled nucleation for the regulation of the particle size in monodisperse gold suspensions. *Nature physical science*, 1973. 241(105): p. 20-22.
26. Park, S., K.A. Brown, and K. Hamad-Schifferli, Changes in oligonucleotide conformation on nanoparticle surfaces by modification with mercaptohexanol. *Nano Letters*, 2004. 4(10): p. 1925-1929.
27. Gerrans, K., et al., Silica nanoparticles functionalized with polyamidoamine (PAMAM) dendrimers as platforms for photoluminescence (PL) sensing of copper and cyanide

ions. *Journal of colloid and interface science*, 2016. 470: p. 276-283.

28. Zhang, X., M.R. Servos, and J. Liu, Ultrahigh nanoparticle stability against salt, pH, and solvent with retained surface accessibility via depletion stabilization. *Journal of the American Chemical Society*, 2012. 134(24): p. 9910-9913.

29. Sun, J., et al., Highly hybridizable spherical nucleic acids by tandem glutathione treatment and polythymine spacing. *ACS applied materials & interfaces*, 2016. 8(19): p. 12504-12513.

30. Hristov, D.R., E. Mahon, and K.A. Dawson, Controlling aqueous silica nanoparticle synthesis in the 10–100 nm range. *Chemical Communications*, 2015. 51(98): p. 17420-17423.

Chapter IV. Development of colorimetric detection method for gliaidn using aptamer based bi-functional linker

IV -1. Introduction

Food allergies are a significant issue worldwide for both food industries and public health [1]. Because no effective cure has been developed for food allergies, avoidance of foods containing allergen(s) is the most appropriate way to prevent reactions or problems. Celiac disease (CD) is an autoimmune pathology triggered by gluten proteins found in food containing wheat, rye, barley, or some oat varieties. Consumption of gluten containing food by celiac people causes the damage of the mucosal villi and can lead to a flattened mucosa, resulting in malabsorption of nutrients and deficiency-related illnesses. In consequence, CD patients, as well as people with other gluten intolerances, must follow a lifelong gluten-free diet. In order to guarantee safety of foodstuff for celiac people, including the so called "sensitive celiac population", the development of inexpensive and rapid methods for gluten determination at low concentration is critical [2, 3].

At present, enzyme-linked immunosorbent assay (ELISA) is the most commonly used method for gluten analysis not only for its selectivity and sensitivity but also for the lack of other reference methods [3-6]. Besides ELISA, other analytical methodologies are currently being developed like mass spectrometry combined with proteomic technologies, methods based on

DNA amplification and electrochemical sensors using as recognition elements molecular imprinted polymers and aptamers [7-17].

In recent decades, many effective techniques have been extensively applied to ensure the proper labelling and management of food allergens, such as gluten. In spite of these various detection methods, a colorimetric detection method for gluten has not been developed yet. This is because gliadin, a quantitative indicator of gluten, is water-insoluble and requires a high dilution factor for detection. Therefore, a colorimetric detection method with a general detection limit of 1 to 100 nM could not detect a sufficiently small concentration of gliadin [18-21].

In this study, effective detection method for gliadin was proposed by introducing a new switchable linker based on aptamer. Unlike existing colorimetric detection methods, proposed colorimetric detection method amplifies the signal through large-scale aggregation and precipitation of gold nanoparticles by introducing the concept of SL. Based on this concept of SL, microorganisms, allergens, and cancer biomarkers have been effectively detected [22-27]. The SL-based detection method developed with the introduction of the new SL effectively detected small amounts of gliadin below the standards for gluten-free foods.

IV-2. Materials and Methods

IV-2.1. Materials

Chloroauric acid and bovine serum albumin (BSA) were purchased from Sigma Aldrich (St. Louis, MO, USA). Tri-sodium citrate was purchased from Yakuri Pure Chemicals Co., Ltd (Kyoto, Japan). Purified natural Ara h 1, biotinylated monoclonal anti-Ara h 1 IgG1 (clone 2F7 C12 D10) antibody, were purchased from Indoor Biotechnologies (Cardiff, UK). LUDOX AS-30 silica (ammonium salt, 30 wt% in water), acetic acid, glutathione, tetrachloroauric(III) acid trihydrate, chloroauric acid and gliadin from wheat were purchased from Sigma Aldrich (St. Louis, MO, USA). Ethyl alcohol was purchased Duksan pure Chemical (Seoul, Korea). Glutaraldehyde and 3-aminopropyltriethoxysilane(APTES) and ethanolamine were purchased from TCI (Tokyo, Japan). ELISA kit to detect gliadin was purchased R-Biopharm AG (Darmstadt,Germany). Gliadin aptamer (5′-(NH_2)-$(CH_2)_6$-TTT TTC TAC ACA TGT CTG AAT GCC-3′) and its part complementary DNA strand (5′-HS-$(CH_2)_6$-TTT TTG GCA TTC AGA CAT GTG TAG-3′.) reported by Svigelj et al. [28] were synthesized by bioneer Coperation (Daejeon, Korea).

IV-2.2. Instrumentation

Absorbance measurements were performed on a UV-1700 spectrophotometer (Shimadzu, Kyoto, Japan). The pH values of all buffer solutions were determined using the Professional Meter PP-15 (Satorious, Göttingen, Germany). Particle sizes and distributions were determined by dynamic light scattering (DLS) with a Zetasizer Nano-ZS 90 (Malvern, Worcestershire, UK). Transmission electron microscopic (TEM) images were obtained using a LIBRA 120 transmission electron microscope (Karl Zeiss, Oberkochen, Germany).

IV-2.3. Preparation of gold nanoparticles (AuNP)

Gold nanoparticles (AuNP), 13 nm in diameter, were synthesised according to the method established by Turkevich et al. [25]. Briefly, the AuNPs were synthesized by adding 5 mL of thrisodium citrate solution (38.8 mM) rapidly to a boiling solution of $HAuCl_4$ (1.0 mM, 50 mL) and stirred for 30 min to form a wine-red solution. Resulting solution was cooled to room temperature while being stirred continuously. Ultimately, AuNP 13 nm in diameter were obtained and stored at 4 °C until further use. All glassware used in the experiment was thoroughly washed with freshly prepared aqua regia

(HNO_3/HCl = 1:3) prior to use. The particle sizes of the AuNP were determined using an ultraviolet/visible (UV/Vis) spectrophotometer and DLS.

IV-2.4. Preparation of aptamer and complementary DNA (cDNA) modified gold nanoparticles

To prepare DNA−AuNP conjugates with the pH-Assisted method, first, various quantity of thiolated DNA stock solution (100 μM in 10 mM Tris-HCl buffer, pH 8.0 with 0.1 mM EDTA) was treated with TCEP (100x) for 1 hr tor cleave the disulfide bond. The resulting solution was added into synthesized AuNP solution (DNA:AuNP ratio = 25:1), and then mixture was heated to 60°C in water bath. Second, pH 3 sodium citrate buffer (100 mM) was introduced to the AuNPs solution with a final concentration of 10 mM. After a 5 min incubation at 60°C temperature, the pH of the AuNP solution was adjusted back to neutral by adding 600 mM HEPES buffer to a final HEPES concentration of 30 mM (pH 7.4). The sample was cooled to room temperature for another 15 min. Finally, the thiol-DNA−AuNPs conjugate was centrifuged at 16,000xg for 30 min, and the supernatant was removed. Finally, the precipitate was washed with 5 mM HEPES to remove free DNA. This centrifugation and washing procedure was repeated 3 times to ensure complete

removal of free thiol-DNA, and the conjugate was kept in 5 mM HEPES buffer for further use.

IV-2.5. Removal of Nonspecific DNA Adsorption on surface of AuNP

Glutathione (GSH) was used to displace the nonspecific adsorption of thiolated DNAs on AuNP surfaces, so as to improve the hybridization capacity of the adsorbed DNA strands with their complementary strands. Glutathione (100 mM) was introduced to the DNA-AuNP conjugate solution with final concentration of 10 mM and incubated for 10 min. Reaction was halted by centrifugation at 16,000xg for 30 min at room temperature. The precipitates were resuspended in 50 mM Tris-HCl buffer (pH 7.4). This centrifugation and washing procedure was repeated 3 times to ensure complete removal of free glutathione, and the conjugate was kept in 50 mM Tris-HCl buffer (pH) with 300 mM NaCl for further use.

IV-2.6. Synthesis of nanoparticles functionalized with amino groups

The method of Gerrans and coworkers was adopted for amino group modifications on Silica nanoparticle [29]. LUDOX AS-30 silica nanoparticles (SNP), 20 mL was added to a solution contacting ethanol (100 mL), water (60

mL) and acetic acid (60 mL). To this solution was added APTES (1.2 mL, 5.2 mmol) followed by stirring at 80°C under N_2 for 48 h. Then, the functionalized silica nanoparticles were isolated by centrifugation (relative centrifugal force, 29,720, 2 h), and the supernatant was decanted, the resulting solid washed with ethanol, and centrifuged again for 2 h. This cycle was repeated thrice more after which the white solids were vacuum dried at 70°C overnight. Finally, the dried SNP-APTES was resuspended in HEPES buffer (20 mM, pH 7.4) for further use.

IV-2.7. Removal of Nonspecific DNA Adsorption on surface of SNP

Glutathione were used to displace the nonspecific adsorption of thiolated DNAs on AuNP surfaces, so as to improve the hybridization capacity of the adsorbed DNA strands with their complementary strands. The synthesized DNA modified SNP nanoconjugates were exposed to glutathione solution (100 mM) were respectively introduced to the DNA-SNP conjugate solution with final concentration of 10 mM and incubated for 10 min. Reaction was halted by centrifugation at 16,000xg for 30 min at room temperature. The precipitates were resuspended in 50 mM Tris-HCl buffer (pH 7.4). This

centrifugation and washing procedure was repeated 3 times to ensure complete removal of free glutathione, and the conjugate was kept in 50 mM Tris-HCl buffer (pH) with 300 mM NaCl for further use.

IV-2.8. Extraction of gliadin

Gliadin fractions were extracted from a rice flour with the procedure described by Mejias et al [30]. Five hundred gram of gliadin from wheat (G3375) was dissolved in 10 mL of 60% (v/v) ethanol, incubated with gentle shaking at 200 rpm for 20 min at room temperature, and centrifuged for 20 min at 10,000xg. The supernatant was recovered, and the gliadin protein concentration was measured using ELISA kit from R-biopharm AG.

IV-2.9. Detection of gliadin in diluted extract solution

The detection system comprised two steps. In the first step, 100 µL of each gliadin extract solution (0, 0.5 µg/mL, 5.0 µg/mL, 50 µg/mL) was mixed with switchable linker (SL) in concentrations ranging from 0.8 mg/mL to 1.2 mg/mL. The mixture was then mildly agitated for 30 min. In the second step, 200 µL of cDNS@AuNP (absorbance of 4.0 at 522.5 ± 0.5 nm) was added and

then agitated for an additional 10 min. The shift in the range exhibiting a visible colour change, which is referred to as the REVC, was identified visually and/or by UV/Vis spectroscopy in the 400–700 nm range.

IV-2.10. Verification of the selectivity of the detection method

One hundred milligram of protein solutions were used in the selectivity tests. Each protein sample was dissolved in 10 mL of 60% (v/v) ethanol extracted in 60%, incubated with gentle shaking at 200 rpm for 20 min at room temperature, and centrifuged for 20 min at 10,000xg. The supernatant was recovered. Each protein was diluted in 50-fold with pH 7.4 of 50 mM Tris-Hcl buffer with 300 mM NaCl. .and then mixed with SL ranging in concentrations from 0.9 mg/mL, 1.0 mg/mL, 1.1 mg/mL. The remaining steps were performed in the manner described above.

IV-2.11. Statistical analysis

The data represent an average of at least three independent experiments or measurements, and the results are expressed as mean ± standard deviation (SD).

IV-3. Results and Discussion

IV-3.1. Hypothesised mechanism for gliadin detection

As shown in Figure IV -1, the proposed method consists of a control line without a target and a test line with a target, and is designed to involve two sequential steps: (1) reaction of the SL (aptamer modified silica nanoparticle) and the target (gliadin), i.e., the target recognition step, and (2) after the reaction time has elapsed, the addition of functionalised AuNP (cDNA@AuNP), i.e., the signal indication step. Two regions can be distinguished in the AuNP/SL aggregates: the REVC with colour change and the region with no colour change (in which the number of linkers that could react with the particles was insufficient or the binding site of the particles were already filled by the linker). The REVC of the control line was determined by the quantitative relationship between the AuNP and SL. In the test line with the target, the SL can be switched off as the SL binds to gliadin, which shifts the REVC to a higher linker concentration range than that of the control line. This colour difference can be used to quantitatively detect the target.

The hypothesised detection mechanism is shown in Figure IV-1, which is based on the change in the aggregation pattern according to the

quantitative correlations among the SL, targets, and AuNP. The SL is an aggregation mediator that can form aggregates with both the targets and AuNP. When the AuNP and SL react at a specific ratio, they form large aggregates, which causes fast precipitation. However, if the target in the sample is preferentially recognised, an SL/target aggregate can form. The resulting aggregate interferes with the formation of AuNP and SL aggregates, which leads to a change in the optimum AuNP/SL ratio for rapid precipitation. Alteration in the precipitation rate of the AuNP/SL aggregates provokes a shift in the visible colour change (REVC) and absorbance in the solution containing them.

The SL used in this study was a crosslinking agent that recognises targets in addition to inducing the large-scale aggregation (aggregates can be precipitated) of AuNP. The SL can induce large-scale aggregations when a specific concentration ratio with AuNP is realized. In addition, when the SL is switched off by a specific target such as gliadin, this specific concentration ratio is readjusted to change the extent of the large-scale aggregation. Unlike colour changes, such as the red and/or blue shift in other colorimetric assays, the colorimetric signal generated by the precipitation of aggregates is more intuitive because the large-scale aggregation reduces the dispersion of AuNP

in the system, such that the colour disappears.

The two-step reaction of this system clearly shows the difference in susceptibility between the gliadin-aptamer interaction in the signal indication step and the streptavidin-biotin binding in the target recognition step. In the gliadin-truncated Gli 4 aptamer and 19-mer of DNA–DNA cases, the equilibrium dissociation constants (K_d) are known to be approximately 10^{-12} M, both of them [31]. However, the difference in the dynamics of these two reactions do not affect the operation of the system, which can be readily explained. First, the system consists of two independent sequential steps (the gliadin- aptamer interaction in the target recognition step and the aptamer–cDNA binding in the signal indication steps). Second, each reaction occurs at a same site but each reaction occurs sequentially to reduce the impact on each other. The reactions are restrictedly competitive. Third, the gliadin/aptamer reaction forms large aggregate before streptavidin/biotin reaction occurs, which results in the rapid formation of large-scale aggregates of AuNP with the SL. These large-scale aggregates then precipitate by gravity depending on their size and density, which results in a visual signal. In this situation, even if the SL is switched on by the reverse reaction of Ara h 1/Ab (such as the SL being detached from the gliadin), it has little chance of reacting with the

aggregates. This process occurs because the larger are the aggregates, the relatively slower is the reaction rate. Gold nanoparticles that do not participate in the formation of aggregates can bind with the switched-on SL, but this process would generate only relatively small-scale aggregates that cannot be precipitated and would be very unlikely to affect the REVC. For these reasons, I believe that the reversibility issue has minimal impact on the sensitivity. In addition, there are some samples for which precipitation occurs slowly depending on the size of the aggregates after the detection time I set (10 min), but this is unrelated to the reversibility.

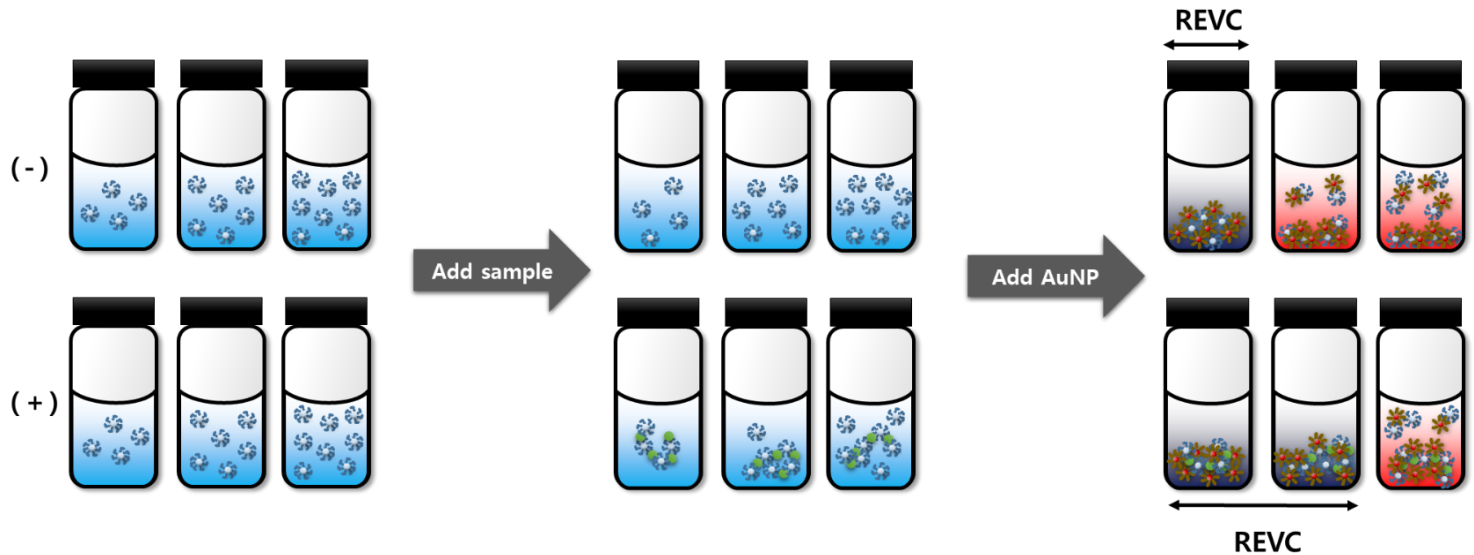

Figure IV-1. Schematic of the colorimetric and visual detection of gliadin based on the shift in the range of the exhibiting visible colour change (REVC). First, aptamer modified silica nanoparticle (the SL) was added to solutions with or without the target (gliadin). Then, complementary DNA modified gold nanoparticles (cDNA@AuNP) were added to the solutions. The target decreased the aggregation capacity of the SL, which caused the AuNP to form an optimal aggregation with a higher SL concentration than that without the target.

IV-3.2. Detection of gliadin in extract solution using the proposed method

Before on-site application, this detection strategy must be optimised in terms of the gliadin-induced REVC shift that is influenced by the concentrations/ratios of SL and cDNA@AuNP. To do so, first, I determined the REVC signal of the control (no target), as shown in Figure IV-2A. This REVC signal was observed at SL concentrations ranging from 0.125 mg/mL to 0.25 mg/mL. And only a slight colour difference (purplish red) was observed at concentrations of 0.0625 mg/mL (low end) and 1.0 mg/mL (high end). This colour difference can be mainly attributed to the surface plasmon resonance (SPR) difference due to the presence of small cDNA@AuNP-SL aggregates that had not yet precipitated. In the treatment of Gliadin (5.0 μg/mL in Figure IV-2A), a right-side REVC shift, as compared with the control REVC, was observed in the SL concentration ranges of 0.25–0.5 mg/mL. This shift of REVC belongs to a small change compared to previous studies using biotin antibody as SL. First of all, this seems to occur because target and complementary DNA compete for the same binding site called aptamer, unlike the existing SL, which used the previously uncompetitive antigen-antibody reaction and biotin-streptavidin reaction as mechanisms. In addition, in the case of the conventional SL, the reaction between streptavidin-biotin was much more preferred than the reaction between antigen-antibody, whereas the

reaction between aptamer-antigen and aptamer-complementary DNA had similar K_d values. The aptamer-antigen response appears to have a less dominant effect.

Then, I further subdivided the SL concentration ranges used for the gliadin detection to obtain a finer and more sensitive quantitative signal change (for example, the REVC shift), from which I determined the SL concentration range to be 0.0625–1.0 μg/mL. As shown in Figure IV-3A, the REVC shift at the low end was less clear than shift at the high end. As a result of DLS anlalysis of the low and high end after the first reaction, it was confirmed that the diameter of SL only increased slightly at the low end, whereas SL and gliadin formed aggregate t the high end (Figure IV-S1A). This causes a relatively large number of gliadins to saturate SL at the low end of a small number of SLs, resulting in the effect of increasing the SL particle itself, whereas at the high end of a large number of SLs, a proper ratio is satisfied to form aggregate between gliadin and SL (Figure IV-S1B). It can be seen that the low end of the form in which gliadin is bound to individual SLs is exposed to conditions that are more likely to compete with complementary DNA in the secondary reaction than the high end of the form in which several particles and gliadin are bound. For this reason, the low end REVC shifting appears to be less than the high end (Figure IV 2B, C, D, E.).

Since the REVC change according to the gliadin concentration in the high end was more easily identified, the subdivision of the SL concentration was selectively conducted only at the high end. The high-end SL concentration interval was divided from 0.8 μg/mL to 1.2 μg/mL by 0.1 μg/mL intervals, and then reacted with SL from 0.5 μg/mL concentration of gliadin to 50 μg/mL concentration of gliadin (Figure IV-5). As a result, the REVC of control appeared only in 0.8 mg/mL of SL Shifting of REVC of 0.5 μg/mL of gliadin was shown to 0.9 mg/mL of SL. And REVC of 5.0 and 50 μg/mL of gliadin was more shifted to higher concentration of SL.

According to the regulation of AOAC, the standard for gluten content in foods that can be recognized as gluten-free foods is 20 mg/kg or less. Of these, gliadin is known to account for half of gluten, and if detection method could measure 10 mg/kg of gliadin, it could tell if it meets the criteria for gluten-free foods. And when gliadin is extracted in 60% ethanol, the dilution factor is 20. Therefore, in order to be recognized that the detection method is suitable for determining gluten-free, it must be possible to determine that the concentration of gliadin in the extract is 0.5 μg/mL or more or less. And this detection system was able to visually detect gliadin with the reference concentration of 0.5 μg/mL.

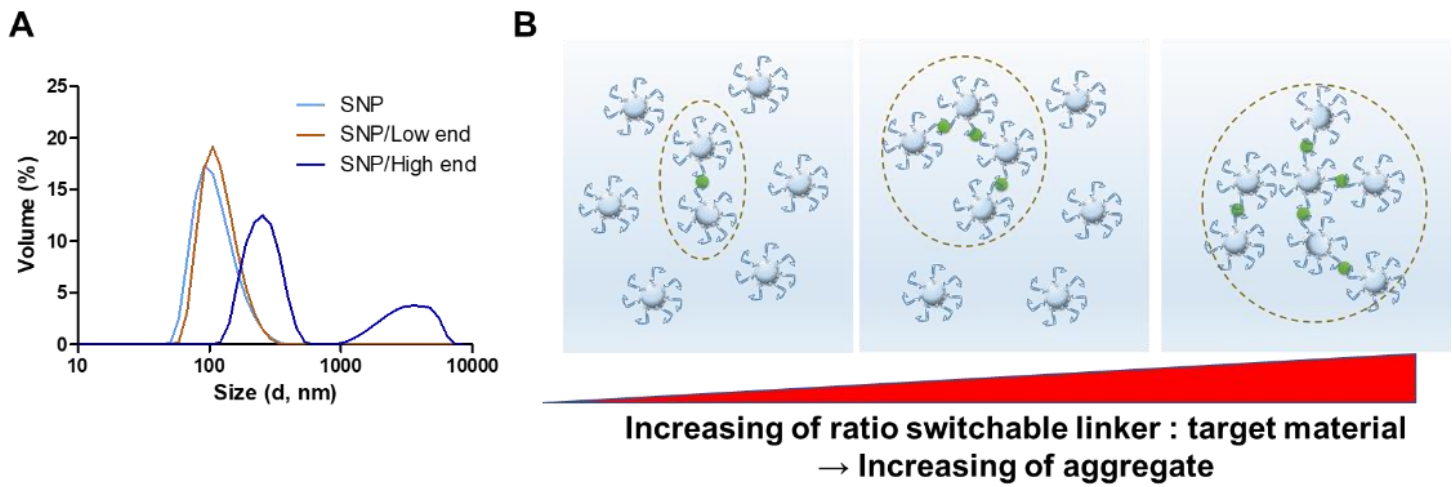

Figure IV-S1. (A) The analysis of aptamer modified SNP physicochemical characteristics was performed by dynamic light scattering (DLS) with/without gliadin and (B) schematic of the size of aggregate according to switchable linker:target material ratio

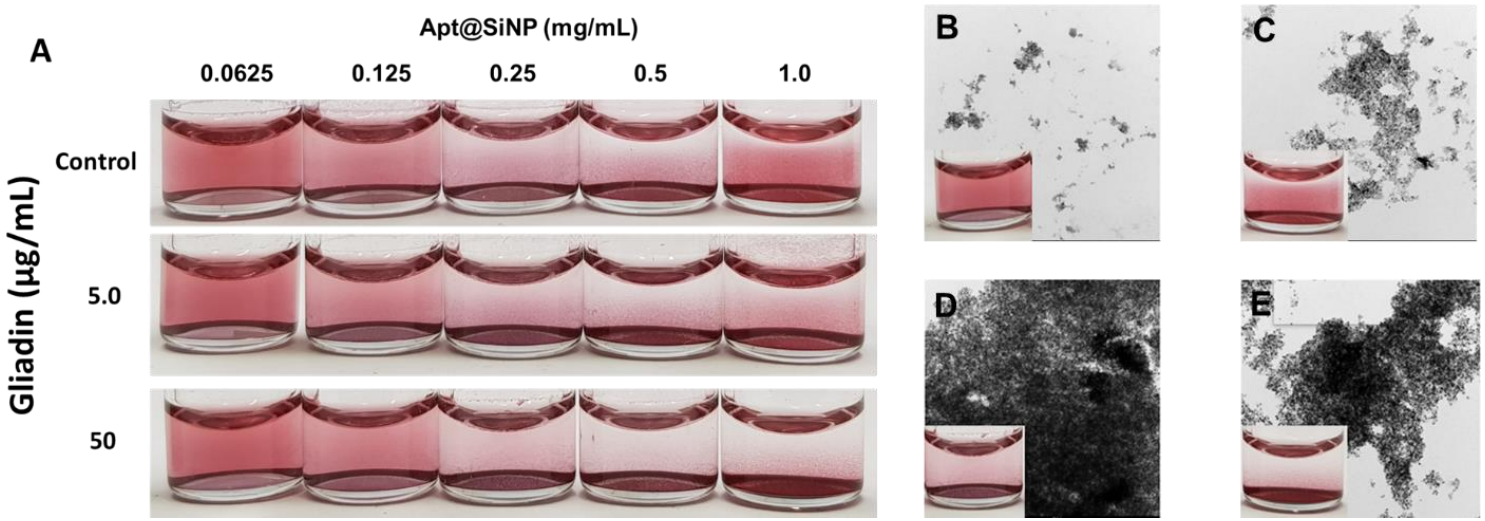

Figure IV-2. (A) Detection of gliadin (0.0, 5.0 µg/mL and 50.0 µg/mL) using the proposed switchable linker (SL)-based assay. Transmission electron micrographs of the gliadin-induced cDNA@AuNP aggregates (B, 0.0625 mg/mL of SL; C, 1.0 mg/mL of SL) at 0.0 µg/mL of gliadin (inset, photograph of their suspensions). (D) Detection of 50.0 µg/mL gliadin (0.25 mg/mL and 1.0 mg/mL) using the proposed SL-based assay.

IV-3.3. UV-Vis spectroscopic approach to gliadin detection

To quantify the visual signal and improve the detection limit of the proposed method, I used a spectrophotometer to analyse the change in absorbance of AuNP aggregates based on the previously mentioned mechanism. The ratio between the AuNP and SL was optimised by testing various concentrations, and finally I identified 1.0 mg/mL of SL, which is a high-end concentration of the control line in Figure IV-3, for use in the experiment. As shown in Figure IV-3, as the concentration of gliadin was increased at a linker concentration of 1.0 mg/mL, the colour change was confirmed as being due to the precipitation of gold aggregates. To confirm the correlation between the colour change and the concentration of gliadin, the change in absorbance was measured. Several gliadin solutions with concentrations between 0.1 μg/mL and 50.0 μg/mL (Figure IV-3) were tested. The changes in absorbance at a peak were found to be significant even with these small amounts of gliadin. I plotted the absorbance at 528 nm with the concentration of gliadin to quantify the change in absorbance (Figure IV-S3). The absorbance at 528 nm was found to be proportional to the concentrations of gliadin in the range from 0.1 μg/mL to 1.00 μg/mL, which can be expressed as a linear equation:

$$A_{528\ nm} = -0.3C_{Gliadin} + 0.8348\ (\mu g/mL) \quad (1)$$

with a correlation coefficient of 0.9941 at $A_{528\ nm}$ for absorbance at 528 nm and $C_{Gliadin}$ for the concentration of gliadin. The linear section (detection range) occurred from 0.1 μg/mL to 1.00 μg/mL, and the slope of the absorbance decreased at higher concentrations (from 1.00 μg/mL to 50.0 μg/mL). Unlike the change in absorbance, almost no shift was observed in the SPR peak (about 6 nm shift) of the small molecule–target AuNP aggregation. Thus, little change in colour was observed. This finding is thought to be the result of interference by silica nanoparticle of the plasmon interactions with AuNP, because silica nanoparticles are relatively larger than AuNP [32]. On the other hand, the speed and size of the AuNP/SL cluster formation were faster and larger than in the conventional AuNP aggregation-based detection method because of the number of aptamer and complementary DNA, which can induce their aggregation on SL and stAuNP surfaces. In addition, core of SL, silica nanoparticle has larger volume and density then protein. Therefore, precipitation of the aggregates occurred within a short time (10 min), and the change in absorbance caused by this precipitation could be measured by a spectrophotometer.

Because AuNP induce colorimetric effects according to the localised surface plasmon resonance (LSPR) principle, nanoparticles in many studies have undergone changes in their size, shape, composition, and interparticle distance [33, 34]. The interparticle distance of AuNP in this system was especially important for inducing the LSPR of AuNP. The silica nanoparticle (26 ± 1.0 nm nm) bigger than AuNP (13 ± 0.5 nm). Therefore, even if cDNA@AuNP-SL aggregates had caused LSPR, the distance between the particles was relatively large, so no dramatic colour changes (red to blue) occurred. In conclusion, when small cDNA@AuNP/SL aggregates were formed, their weak colour changes via SPR could have occurred with a small peak shift (6 nm).

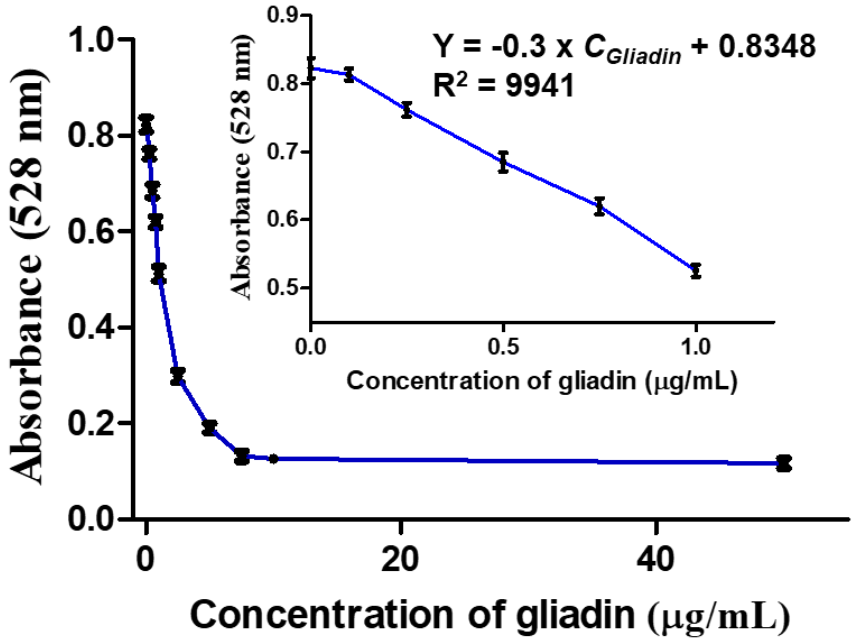

Figure IV-3. Ultraviolet/visible (UV/Vis) spectroscopy analysis. a plot of the absorbance at 528 nm versus the gliadin concentration (inset, magnified linear region). All analyses were conducted on samples with an SL concentration of 1.0 mg/mL.

IV-3.4. Selectivity of the detection method

To determine the selectivity of the SL-based colorimetric detection system with respect to gliadin, I used the proposed method to test gliadin extracts and four other sample (Bovine serum albumin, streptavidin, Ara h1, Anti-Ara h 1 antibody). As shown in Figure IV-4A, the REVC of the gliadin extract shifted and precipitation occurred in the selected linker concentrations (from 0.9 mg/mL to 1.1 mg/mL). However, all the other extracts exhibited an REVC similar to that of the control sample. In addition, as shown in Figure IV-4B, if I compare the absorbance of each sample at a 1.0 mg/mL linker concentration, the significant difference in the visual effect of the gliadin test group compared to the other test groups is confirmed.

In this study, gliadin was successfully detected in a colorimetric detection system utilizing a aptamer based bifunctional linker without an analytical instrument. The amount of gliadin detected was small enough to be certified as gluten free. However, in this study, detection was performed to purified gliadin extracted from the crude protein, rather than hazard detection in real food. When detecting gliadin in real foods, it can exhibit lower selectivity sensitivity due to interference with various substances such as carbohydrates, fatty acids, tannins, etc. Therefore, in order to take advantage of the success of the detection system, further research is needed

to confirm whether the detection system works properly for various real foods.

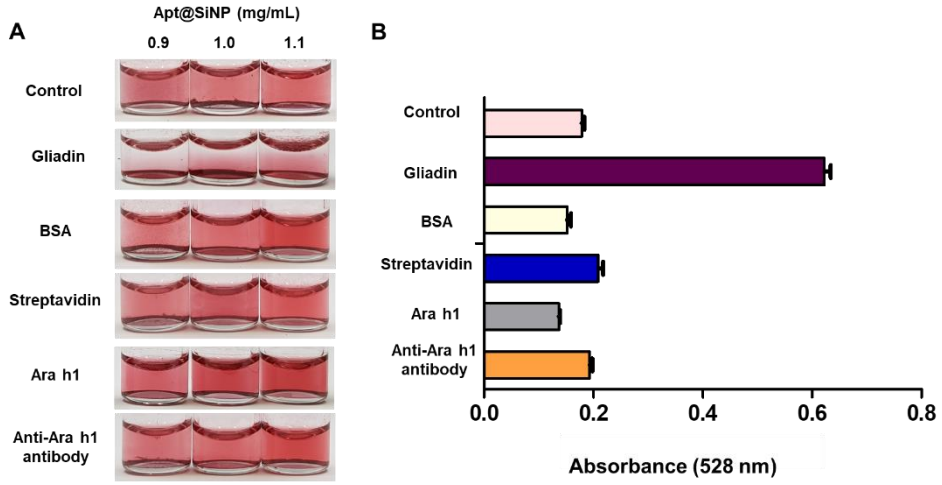

Figure IV-4. Selectivity of the proposed SL-based colorimetric detection system. (A) The high-end REVC for detection with the solutions extracted from gliadin powder and several proteins (bovine serum albumin, streptavidin, Ara h 1, Anti-Ara h1 antibody) (B) Comparison of absorbance at 528 nm of each sample with a aptamer modified SNP concentration of 1.0 mg/mL. Control was a 50 mM Tris-Hcl buffer with 300 mM NaCl (pH 7.4)

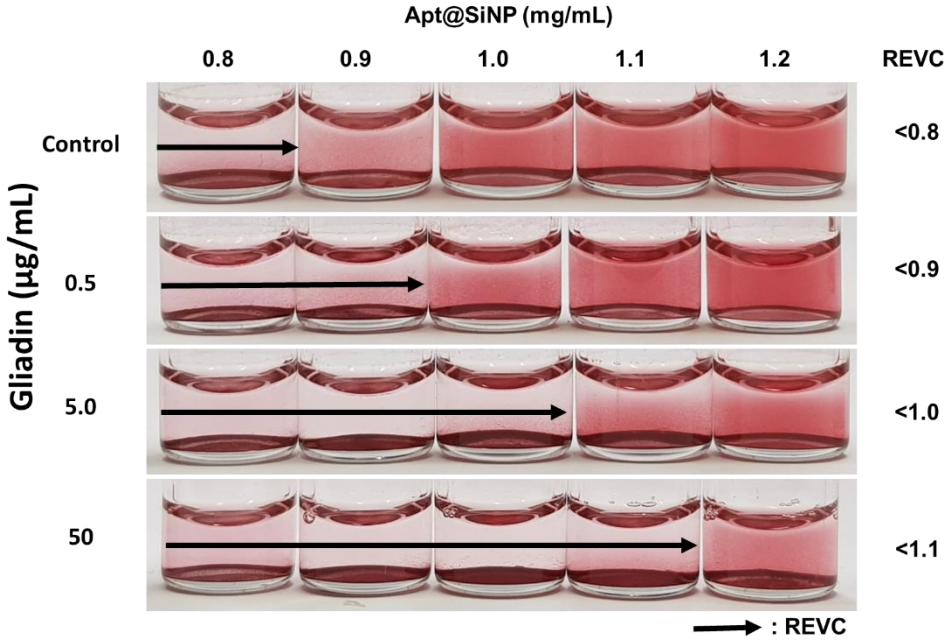

Figure IV-5. Shift in the high-end REVC in response to the presence of gliadin 0.5, 5.0 and 50 µg/mL peanut protein (A) and 0.19 mg and 1.9 mg peanut protein

IV-4. Conclusions

Gluten is a protein commonly found in many foods, but it is also a contributor to celiac disease in certain people. For these people, over the years, rapid detection methods have been developed that can discriminate between gluten-free foods and whether they contain gluten. The colorimetric detection method, despite its simplicity and rapidity, did not meet the increased sensitivity due to the high dilution factor due to alcohol-based extraction, and thus was not applied to the development of a gluten detection method. In this study, I introduced a switchable linker based on aptamer and proposed a colorimetric detection method based on gold nanoparticle precipitation. Gold, which replaces the existing antibody-based SL, introduces silica nanoparticles decorated with aptamers that specifically recognize to gliadin, a constituent of gluten, into SL, and forms complementary DNA that complementarily binds to the aptamers. A colorimetric detection method was developed by using nanoparticles as a probe to form large-scale aggregates and precipitate them. When the SL was introduced, the degree of sedimentation was sensitively changed because the formation of aggregates with gold nanoparticles was disturbed at the high end where the targets gliadin and SL form large-scale aggregates. Using such characteristics, it was possible to detect gliadin less

than 0.5 μg/mL visually without analysis equipment, which satisfies the level of classifying gluten-free foods and it was shown good selectivity.

In this study, gliadin was successfully detected in a colorimetric detection system utilizing a aptamer based bifunctional linker without an analytical instrument. The amount of gliadin detected was small enough to be certified as gluten free. However, in this study, detection was performed to purified gliadin extracted from the crude protein, rather than hazard detection in real food. When detecting gliadin in real foods, it can exhibit lower selectivity sensitivity due to interference with various substances such as carbohydrates, fatty acids, tannins, etc. Therefore, in order to take advantage of the success of the detection system, further research is needed to confirm whether the detection system works properly for various real foods. Although problems such as the simplification and automation of detection must be solved for field applications, SL-based assays provide visibility of results, time efficiency, and ease-to-use that are suitable in the field while also representing a promising alternative for the detection of other proteins and biomaterials in food.

IV-5. References

1. Verhoeckx, K.C., et al., Food processing and allergenicity. *Food and Chemical Toxicology*, 2015. 80: p. 223-240.
2. Amigo, C.D. and B. Popping, Labeling regulations, detection methods, and assay validation. *Journal of AOAC International*, 2012. 95(2): p. 337-348.
3. Diaz-Amigo, C. and B. Popping, Accuracy of ELISA detection methods for gluten and reference materials: a realistic assessment. *Journal of agricultural and food chemistry*, 2013. 61(24): p. 5681-5688.
4. Gagnon, P., et al., Transient conformational modification of immunoglobulin G during purification by protein A affinity chromatography. *Journal of Chromatography A*, 2015. 1395: p. 136-142.
5. Holzhauser, T., et al., Are current analytical methods suitable to verify VITAL® 2.0/3.0 Allergen Reference doses for EU Allergens in Foods? *Food and Chemical Toxicology*, 2020: p. 111709.
6. Iqbal, A., et al., Allergens of Arachis hypogaea and the effect of processing on their detection by ELISA. *Food & nutrition research*, 2016. 60(1): p. 28945.
7. Gezer, P.G., G.L. Liu, and J.L. Kokini, Development of a biodegradable sensor platform from gold coated zein nanophotonic films to detect peanut allergen, Ara h1, using surface enhanced raman spectroscopy. *Talanta*, 2016. 150: p. 224-232.

8. Huang, Y., M.C. Bell, and I.I. Suni, Impedance biosensor for peanut protein Ara h 1. *Analytical chemistry*, 2008. 80(23): p. 9157-9161.

9. Huang, Y. and I.I. Suni, Degenerate Si as an electrode material for electrochemical biosensors. *Journal of The Electrochemical Society*, 2008. 155(12): p. J350.

10. Miyazaki, A., et al., Real-time PCR detection methods for food allergens (wheat, buckwheat, and peanuts) using reference plasmids. *Journal of agricultural and food chemistry*, 2019. 67(19): p. 5680-5686.

11. Puente-Lelievre, C. and A.C. Eischeid, Development and evaluation of a real-time PCR multiplex assay for the detection of allergenic peanut using chloroplast DNA markers. *Journal of agricultural and food chemistry*, 2018. 66(32): p. 8623-8629.

12. Sheu, S.-C., et al., Development of loop-mediated isothermal amplification (LAMP) assays for the rapid detection of allergic peanut in processed food. *Food chemistry*, 2018. 257: p. 67-74.

13. Singh, H., et al., Standardization of RP-HPLC methods for the detection of the major peanut allergens Ara h 1, Ara h 2 and Ara h 3. *Food chemistry*, 2016. 194: p. 383-390.

14. Sobhan, A., et al., Assessment of peanut allergen Ara h1 in processed foods using a SWCNTs-based nanobiosensor. *Bioscience, Biotechnology, and*

Biochemistry, 2018. 82(7): p. 1134-1142.

15. Sun, X., et al., Electrochemical detection of peanut allergen Ara h 1 using a sensitive DNA biosensor based on stem–loop probe. *Journal of agricultural and food chemistry*, 2012. 60(44): p. 10979-10984.

16. Tran, D.T., et al., Selection of aptamers against Ara h 1 protein for FO-SPR biosensing of peanut allergens in food matrices. *Biosensors and Bioelectronics*, 2013. 43: p. 245-251.

17. Trashin, S., et al., Label-free impedance aptasensor for major peanut allergen Ara h 1. *Electroanalysis*, 2015. 27(1): p. 32-37.

18. Chen, H., K. Zhou, and G. Zhao, Gold nanoparticles: From synthesis, properties to their potential application as colorimetric sensors in food safety screening. *Trends in Food Science & Technology*, 2018. 78: p. 83-94.

19. Fang, C., et al., Gold nanoparticle-based optical sensors for selected anionic contaminants. *TrAC Trends in Analytical Chemistry*, 2017. 86: p. 143-154.

20. Hristov, D.R., E. Mahon, and K.A. Dawson, Controlling aqueous silica nanoparticle synthesis in the 10–100 nm range. *Chemical Communications*, 2015. 51(98): p. 17420-17423.

21. Jazayeri, M.H., et al., Colorimetric detection based on gold nano particles (GNPs): An easy, fast, inexpensive, low-cost and short time method in detection of analytes (protein, DNA, and ion). *Sensing and bio-sensing*

research, 2018. 20: p. 1-8.

22. Hahn, J., et al., Development of a portable lab-on-a-valve device for making primary diagnoses based on gold-nanoparticle aggregation induced by a switchable linker. *RSC Advances*, 2020. 10(52): p. 31243-31250.

23. Hahn, J., et al., Colorimetric switchable linker-based bioassay for ultrasensitive detection of prostate-specific antigen as a cancer biomarker. *Analyst*, 2019. 144(14): p. 4439-4446.

24. Hahn, J., et al., A Switchable Linker-Based Immunoassay for Ultrasensitive Visible Detection of Salmonella in Tomatoes. *Journal of food science*, 2017. 82(10): p. 2321-2328.

25. Kim, E., et al., Visible on-site detection of Ara h 1 by the switchable-linker-mediated precipitation of gold nanoparticles. *Food Chemistry*, 2021. 352: p. 129354.

26. Lim, S., et al., Enhancing nanoparticle-based visible detection by controlling the extent of aggregation. *Scientific reports*, 2012. 2(1): p. 1-6.

27. You, Y., et al., Bifunctional linker-based immunosensing for rapid and visible detection of bacteria in real matrices. *Biosensors and Bioelectronics*, 2018. 100: p. 389-395.

28. Svigelj, R., et al., Truncated aptamers as selective receptors in a gluten sensor supporting direct measurement in a deep eutectic solvent. *Biosensors and*

Bioelectronics, 2020. 165: p. 112339.

29. Gerrans, K., et al., Silica nanoparticles functionalized with polyamidoamine (PAMAM) dendrimers as platforms for photoluminescence (PL) sensing of copper and cyanide ions. *Journal of colloid and interface science*, 2016. 470: p. 276-283.

30. Mejías, J.H., et al., Analysis of wheat prolamins, the causative agents of celiac sprue, using reversed phase high performance liquid chromatography (RP-HPLC) and matrix-assisted laser desorption ionization time of flight mass spectrometry (MALDI-TOF-MS). *Nutrients*, 2014. 6(4): p. 1578-1597.

31. Wang, C., et al., Kanamycin detection based on the catalytic ability enhancement of gold nanoparticles. *Biosensors and Bioelectronics*, 2017. 91: p. 262-267.

32. Sendroiu, I.E., S.F. Mertens, and D.J. Schiffrin, Plasmon interactions between gold nanoparticles in aqueous solution with controlled spatial separation. *Physical Chemistry Chemical Physics*, 2006. 8(12): p. 1430-1436.

국문 초록

식품산업에서 식품내 여러 위해요소의 신속한 검출의 중요성은 식품산업의 성장과 함께 커지고 있다. 현재 여러 분석법이 위해요소 검출에 사용되고 있지만, 식품산업은 저숙련 노동자가 많이 종사하고있고 부가가치가 상대적으로 낮은 산업에 속하기 때문에 더 쉽고, 더 간편하고, 더 저렴한 신속검출법의 개발이 여전히 필요하다.

금 나노입자 응집기반 비색검출법은 금 나노입자가 가시광선을 흡수하는 특성을 이용하기 때문에 특별한 분석장비 없이 눈으로도 검출 결과를 확인할 수 있다는 장점이 있다. 또한 금 나노입자는 저렴하게 제작이 가능하기 때문에 식품 내 위해요소 신속검출법 개발에 활용되기 적합하다. 하지만 금나노입자 응집 기반 비색검출법은 분석장비를 활용하는 전기적 또는 광학적 분석법보다 검출한도가 낮으며, 식품처럼 여러 물질이 혼합된 시료에서는 높은 선택성을 가지는 검출 시스템을 구축하는 것이 어렵다는 단점이 있다. 이러한 금나노입자를 활용한 비색검출법의 단점을 극복

하기 위해, 금나노입자의 대규모 응집을 유도하여 신호를 증폭하는 동시에 선택적인 검출 대상 인지가 가능한 이중기능링커를 활용한 금나노입자 응집기반 신속 검출법에 대한 연구가 진행되고 있다. 하지만 아직 대부분의 연구가 미생물 검출에 한정되어 있으며 항체 기반 이중기능링커를 사용해야하기 때문에 한정된 확장성을 지니는 단점이 존재한다.

본 논문에서는 이러한 이중기능링커 활용의 어려움들을 극복하고자 하였다. 먼저, 금 나노입자의 응집반응으로 땅콩 알러젠인 Ara h1을 실제 식품인 쿠키에서 알러지 환자가 인지할 수 있는 최소한도인 ED01 기준치 이하로 신속히 검출하는 연구를 수행하였다. 추출시간을 포함하여 45분 이내에 0.19 mg/mL 이하의 땅콩 단백질을 검출할 수 있음을 보임으로서 이중기능링커 기반의 검출 시스템이 기존의 미생물뿐만 아니라 다른 위해물질 검출에도 적용될 수 있음을 보였다. 두번째로 압타머 기반 이중기능링커와 금나노입자 표면 개질법을 고안하여 새로운 형태의 이중기능링커 기반 신속검출법을 개발하는 연구를 수행하였다. 항체와 같이 특정 단백질을 인지할 수 있는 기능이 있는 DNA 서열인 압타머(Aptamer)를

실리카 나노입자에 표면에 성형하고 이에 상보적인 DNA 서열을 금나노입자 표면에 성형함으로써 항체 없이도 타겟 물질 인지와 금나노입자 응집유도가 가능한 이중기능링커와 이를 활용한 응집 시스템을 고안하였다. 마지막으로, 압타머 기반 이중기능링커를 활용하여 셀리악 병의 원인 물질인 gliadin을 신속하게 검출하는 연구를 수행하였다. 새로 개발된 이중기능링커 기반 비색검출법을 활용하여 0.5 μg/mL 이하의 gliadin을 분석도구 없이 눈으로 검출할 수 있었다. 새로 개발된 압타머 기반 이중기능링커와 이를 활용한 신속검출법은 아직 연구되어야 할 부분이 많이 남아있지만 이를 활용하여 보다 다양한 식품 내 위해요소를 대상으로 이중기능링커 기반 신속검출법을 확장 적용할 수 있을 것이라 기대된다.

핵심어: 금 나노입자(Au NP), 실리카 나노입자 (SNP), 이중기능링커 (SL), 압타머 (Aptamer)

학 번: 2016-39133